# Dipolar interactions and hydrogen bonding in supramolecular aggregates: understanding cooperative phenomena for 1st hyperpolarizability

**Ayan Datta and Swapan K. Pati***

***Received 7th August 2006***
***First published as an Advance Article on the web 13th October 2006***
**DOI: 10.1039/b605478a**

Weak intermolecular forces like dipolar interactions and hydrogen-bonding lead to a variety of different packing arrangements of molecules in crystals and self-assemblies. Such differences in the arrangements change the extent of excitonic splitting and excitation spectra in the multichromophore aggregates. In this *tutorial review*, the role of such interactions in fine tuning the linear and 1st non-linear optical (NLO) responses in molecular aggregates are discussed. The non-additivity of these optical properties arise specifically due to such cooperative interactions. Calculations performed on dimers, trimers and higher aggregates for model systems provide insights into the interaction mechanisms and strategies to enhance the 1st hyperpolarizabilities of π-conjugated molecular assemblies. Flexible dipole orientations in the alkane bridged chromophores show odd-even variations in their second-harmonic responses that are explained through their dipolar interactions in different conformations. Parameters for the optical applications of molecules arranged in constrained geometry, like in Calix[n]arene, have been elucidated. We also highlight the recent developments in this field of research together with their future prospects.

## 1 Introduction

Materials exhibiting large non-linear optical (NLO) properties are gaining prominence in basic as well as industrial research due to their applications in many opto-electronics devices.[1,2] Such materials exhibit exotic properties such as second harmonic generation (SHG), optical rectification (OR),

*Theoretical Sciences Unit, Chemistry and Physics of Materials Unit and DST Unit on Nanoscience, Jawaharlal Nehru Center for Advanced Scientific Research, Jakkur Campus, Bangalore 560 064, India. E-mail: pati@jncasr.ac.in*

**Ayan Datta**

*Ayan Datta was born in West Bengal, India, in 1980. He completed his bachelors degree with chemistry honours from Calcutta University in 2001 and joined for the integrated PhD programme in Jawahalal Nehru centre for advanced scientific research, Bangalore in the same year. He completed his PhD in 2006 working under the guidance of Prof. Swapan K. Pati on theoretical chemistry. His research interests include quantum chemistry and statistical mechanics for applications in non-linear optical responses of molecules and extended systems, stability of nanoclusters, magnetism at all length scales and electron and proton-transfer processes in the interface of physics, chemistry and biology. He is also greatly interested in writing popular science articles and designing tool-kits and software for chemical education.*

**Swapan K. Pati**

*Swapan K. Pati had his early education at the Midnapore College and at Kalyani University, West Bengal. He finished his PhD from the Indian Institute of Science, Bangalore followed by postdoctoral work in the department of physics at University of California, Davis, and in the chemistry department at Northwestern University. He is currently an associate professor at the Jawaharlal Nehru Centre for advanced scientific research, Bangalore. He is a junior associate of the Abdus Salam International Centre for Theoretical Physics, Italy, since 2003. He has been a visiting faculty member to Purdue University, the University of Tokyo and the Max Planck Institute for Physics of Complex systems, Dresden. He is a recipient of the bronze medal from the Material Research Society of India (2006). His research interests include quantum many-body theory, molecular electronics, non-linear optical phenomena, quantum magnetism and generalized charge-transfer mechanisms. He is also actively involved in developing new theoretical tools for a holistic understanding of structure–property correlations in a whole range of systems from molecules to materials including biological and bio-mimetic systems (see http://www.jncasr.ac.in/patil for more information).*

multi-photon processes and coherent anti-stokes Raman scattering (CARS), to name a few.[3] A major push towards molecular and polymer materials have been the outcome of the impressive growth in the industrial applications of polymeric conductors and light emitting diodes.[4] Along with the direct NLO applications of π-conjugated systems, there has been a tremendous interest for basic research on materials for large NLO properties.[5–9] This is clearly seen in Fig. 1(a) showing a leap in the number of publications in this area for the last decade. Even more encouraging is the exponential increase in the number of reports in chemistry journals in this area in the last 5 years (Fig. 1(b)). On the experimental front, much of these efforts are directed towards synthesis, characterization and crystallization of new NLO active molecules, polymers and self-assemblies for a wide variety of applications.[10–12]

Theoretical modeling of NLO active chromophores and the *a priori* prediction of the response functions in technologically important classes of materials has been on the rise. Many groups around the world have contributed substantially to this growth, which is ever increasing. To name a few prominent contributions, for example, M. Ratner and T. J. Marks *et al.* have calculated NLO responses in the π-stacked dimers of paranitroanilines, dimers of triazene–vinylbenzylidene–barbituric acids and on 7,7-dipyrrolidine-8,8-dicyanoquinodimethane (DPDQ).[13] The role of intermolecular H-bonding interactions and dipolar coupling have been discussed within the framework of the exciton model. Peris and co-workers have considered the head-to-tail arrangement of paranitroaniline and their calculations have shown large cooperative enhancements in the molecular second-harmonic generation

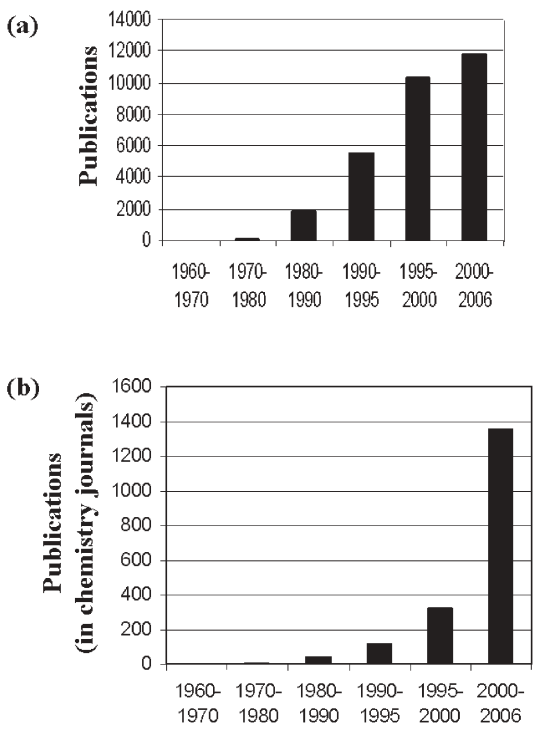


**Fig. 1** (a) Total number of papers published with 'Nonlinear Optics' keywords. (b) Papers published in chemistry journals with 'Nonlinear Optics' keywords. Data derived from SCOPUS search (Elsevier B.V.).

(SHG) coefficients ($\beta$). They have also considered chains of HF molecules in both their linear and zig-zag orientations wherein they find cooperative enhancement of $\beta$ for the linear chains and cooperative damping in the zig-zag chains.[14] Wu and co-workers have studied chains of urea molecules up to septamers and their calculations show that intermolecular H-bonding are significant for $\beta$ and proper inclusion of electron correlations at the Møller–Plesset 2 (MP2) level lead to enhancement of 15 percent in $\beta$ from the additive values as derived from the oriented gas-model.[15] However, calculations on the H-bonded dimers of aromatic carboxylic acids with various donor functionalizations and also nitro-amine dimers by Sarma *et al.* show that the extent of intermolecular interactions due to H-bonding does not lead to cooperative NLO properties.[16] Champagne and co-workers have performed calculations on the crystals of 3-methyl-4-nitroaniline (MNA) wherein they find that such crystals show very strong anisotropy in polarization along the three crystallographic axes.[17] For the long axis, where the molecules are arranged in head-to-tail fashion, H-bonding leads to enhanced electrostatic interactions as a consequence of which the transition dipole moment to the charge transfer states increases. This enhances only one diagonal component of $\beta$. However, such interactions being absent in the other two directions, lead to reduction in $\beta$ along these axes. The methodology of calculations of hyperpolarizability in the crystals has also been reviewed.[18]

Apart from calculations on the aggregate, a major impetus of current research is directed towards development of new computational techniques for calculation of the NLO responses. Jensen *et al.* have developed a dipole-interaction model for calculation of polarizabilities in large aggregates of molecular clusters wherein the responses of aggregates as large as 300 molecules can be determined. Their results compare fairly well with *ab initio* calculations.[19] Dykstra *et al.* and Maraoulis *et al.* have performed *ab initio* calculations with varying levels of electron correlations and basis sets to account for accurate calculations of NLO responses in molecular systems.[20] Pati *et al.* have developed a theory based on the density-matrix renormalization group (DMRG) technique to accurately calculate the dynamic NLO responses in model π-conjugated systems.[21]

As a whole, from the technology point of view, the synthesis of newer crystals with large NLO activity requires an understanding of the processes involved in crystallization together with the forces that stabilize non-centric arrangement of molecules in the crystals and self-assemblies. Recent combined experimental and theoretical work by Custelcean *et al.* investigates the role of the steric interactions of the alkyl groups in *N,N*-dialkylthioureas in fine-tuning the H-bonding interactions in the crystalline environment.[22] Lee *et al.* have performed density functional theory calculations for the charge-density and topological feature like atoms-in-molecules (AIM) on the monomers, dimers, heptamers and X-ray structures of thiourea *S,S*-dioxide, to understand the intermolecular charge density distributions for different sizes of the aggregates.[23]

From the discussion above, it is quite clear that for the design of smart materials for large NLO responses one needs to understand the nature of intermolecular forces from an

 

atomistic point of view. This review provides a comprehensive detail of the essential theoretical framework involved in the computations. Followed by this, strategies are proposed for collective enhancement of NLO responses in assemblies and molecular systems. The theoretical models are tested on experimentally synthesized systems wherever the crystal structure or solution measurements of $\beta$ are available.

## 2 Exciton model for molecular aggregates

### 2.1 Dipolar interactions

In this section we discuss a basic model which can explain the electronic excitations of one-dimensional (1-D) molecular aggregates.[24,25] As it is quite well known in the field of strong correlations, an excitonic state is the result of electron correlation and exciton theory is an interaction theory between these excitonic states.[26,27] In self-assembled aggregates with low packing densities, the excitons are considered to be Frenkel type excitons where the electron and hole of a mono-excitation are located on the same molecular site. To develop a simple theory, one considers composite molecules, that include van der Waals dimers, trimers and higher order aggregates. As has been pointed out in a number of previous papers,[28,29] if the direct overlap between the chromophoric molecular orbitals (M.O.) is negligible, the exciton interactions can be expressed in the direct product basis of the chromophoric M.O.s.

Let us begin our discussion with the zeroth order Hamiltonian. The Hamiltonian for the $m$th molecule alone in an aggregate can be written as

$$H_m = \sum_k |k_m\rangle (E^{k,m}) \langle k_m| \tag{1}$$

where $k_m$ specifies the $k$th electronic state of the $m$th molecule. The wavefunction for the $N$ number of molecules (in an aggregate) can be approximated as a linear combination of product functions $|k_1,k_2,\ldots,k_m,\ldots,k_N\rangle$ where the $k_m$'s are the $k$th electronic states for the molecule $m$. If one includes the electronic exchange interactions, the excitations will be the admixtures of charge transfer states which correspond to Wannier type excitons. However, it is explicitly assumed that the intermolecular distance is large enough to make electron exchange effects quite negligible, at least in low order. The ground state of $N$ molecules is then the tensorial product of the molecular ground states.

$$|G\rangle = |G_1,\ G_2,\ldots,\ G_m,\ldots,\ G_N\rangle \tag{2}$$

Each molecular excitation gives rise to a band of $N$ degenerate product states in the zeroth order. For excitation $e$ in the $m$th molecule, it reads

$$|m,e\rangle = |G_1,\ G_2,\ldots,G_{m-1},e_m,G_{m+1},\ldots,G_N\rangle \tag{3}$$

In general, the spatial structure of an aggregate is not quite well defined. However translational symmetry can be assumed to be valid in case of a molecular crystalline system. Herein, we consider the cases of perfect molecular aggregates with no disorder. The exciton coupling interaction term is denoted as $H_{m,n}$ for the interaction between the monomer $m$ and $n$. We derive the energy expression with the general $H_{m,n}$ terms now and introduce the particulars about this interaction later. For the $N$ monomeric molecules, energy matrix for any excitation $e$, for the perturbation $H_{m,n}$ will have the general form

$$[E_{mn}] = E_G(N-1) + \begin{bmatrix} E_e & H_{1,2} & H_{1,3} & \ldots & H_{1,N} \\ H_{2,1} & E_e & H_{2,3} & \ldots & H_{2,N} \\ H_{3,1} & H_{3,2} & E_e & \ldots & H_{3,N} \\ \vdots & \vdots & \vdots & \vdots & \vdots \\ H_{N,1} & H_{N,2} & H_{N,3} & \ldots & E_e \end{bmatrix} \tag{4}$$

where $E_G$ and $E_e$ are the ground state energy and energy for the excitation $e$ respectively. The matrix is assumed to be symmetric so that $H_{m,n} = H_{n,m}$.

For dipolar molecules, the strongly allowed transition would be to the lowest exciton state and the coupling interactions can be approximated at large distances by a point dipole model. The coupling interactions can be written as[30]

$$H_{m,n} = \frac{\overrightarrow{M}_{gs}^{(1)} \cdot \overrightarrow{M}_{gs}^{(2)}}{r_{mn}^3} - \frac{3\left(\overrightarrow{M}_{gs}^{(1)} \cdot \overrightarrow{r}_{mn}\right)\left(\overrightarrow{M}_{gs}^{(2)} \cdot \overrightarrow{r}_{mn}\right)}{r_{mn}^5} \tag{5}$$

where $\overrightarrow{M}_{gs}^{(1)}$ and $\overrightarrow{M}_{gs}^{(2)}$ are the transition moments from state $g$ to state $s$ of the two monomer molecules respectively and $r_{mn}$ is the distance between the two molecular centers $m$ and $n$. It is to be noted that both the transition dipole and the molecular axis ($\overrightarrow{r}_{mn}$) are vectorial quantities. Thus the magnitude of the interaction term will depend crucially on the relative orientations of the dipolar molecules as well as on the axis joining their centers. This is a purely quasi-classical vector treatment and only electrostatic interactions are considered between the transition moments.

A number of cases can be analyzed for dipolar molecules arranged in various orientations. Depending on the orientation of the dipoles, the interactions in an aggregate will be governed uniquely by the angle between the two dipoles ($\phi$) and the angles that the dipolar axes make with each of the molecular axes ($\theta_1$ and $\theta_2$). It is quite simple to derive the splitting energy in such cases from eqn (5),

$$\Delta E = 2\frac{M_{gs}^{(1)} \cdot M_{gs}^{(2)}}{r_{mn}^3}(\cos\phi - 3\cos\theta_1\cos\theta_2) \tag{6}$$

Therefore a singlet excited state of the monomer molecule would split according to the angles, ($\theta_1$, $\theta_2$, $\phi$). In Fig. 2, we show the splitting patterns for representative ideal cases of 1-D molecules for which the dipolar axes and the molecular axes coincide ($\theta_1$, $\theta_2$ = 0,0). On the formation of the head-to-tail arrangement of a dimer ($\phi$ = 0 as shown in Fig. 2(a)), the ground state is stabilized due to favorable dipole–dipole attraction while the excited state splits into two states. Since, dipolar interaction is attractive for this case, the dipole-allowed transition occurs from the ground state to the lower excited state, while transition is forbidden to the higher excited state. Clearly, the transition energy is smaller than the gap for the monomers and thus this mode of aggregation leads to red-shift in the adsorption spectra. For the case of repulsive dipolar interactions ($\phi$ = 180) as shown in Fig. 2(b), the ground state is destabilized, while the excited state splits into two

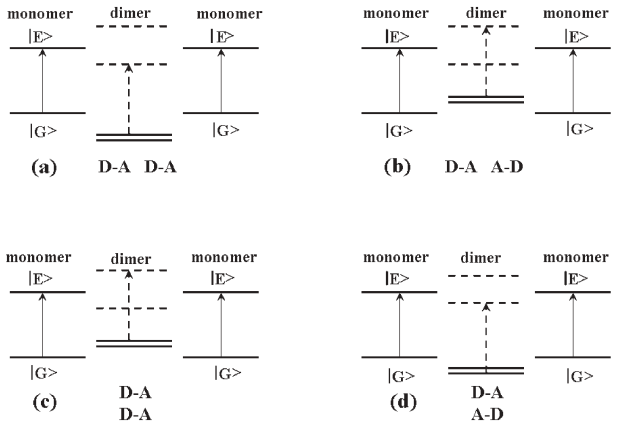


**Fig. 2** Orientations of the monomer dipoles in a composite system, with D–A representing dipolar axis. Each molecule has two levels $|G\rangle$ and $|E\rangle$ and the arrows between states indicate the allowed transitions. The excited states of the composite system are denoted as dashed lines and the allowed transitions are shown by dashed arrows.

states, with the allowed transition occurring from the ground state to the higher excited state. Since this involves larger energy the spectra will be blue shifted.

Apart from the linear arrangement of the dipoles, very common orientation of dipoles are the parallel ($\phi$ = 90) and anti-parallel ($\phi$ = 270) stacking arrangements. They are shown schematically in Fig. 2(c) and Fig. 2(d) respectively. For the parallel arrangement [Fig. 2(c)], the ground state of the dimer is destabilized due to unfavorable dipole–dipole repulsion while the excited state splits into two states. However, now due to dipole–dipole repulsion, the dipole allowed transition occurs from the ground state to the higher excited state. For the anti-parallel arrangement, the ground state as well as the lower excited state are stabilized and thus the dipole allowed transition occurs from the ground state to the lower excited state. Other than the ideal cases shown in Fig. 2, for intermediate angular orientations (different $\phi$ and $\theta_1$, $\theta_2$) of the dipoles, it becomes fairly simple to find the excitation spectra for the dimers using the above formalism. Note that for such cases, both the excited states become accessible from the ground state, with varying oscillator strengths depending on the transition electric dipoles.

### 2.2 Polar and polarizable chromophores

The excitonic model discussed above takes into account the gross interactions among the dipolar molecules. However, a major limitation of this theory is that it does not consider explicit electrostatic interactions among the monomers. To be precise, though the molecules are polar, within the framework of the excitonic coupling theory, the charge density on the atoms in the aggregate do not reorganize due to excitation in a single monomer. Thus, even though the molecules are polar, they are not polarizable due to the internal electric field within the aggregates. Introducing polarizability within the chromophores due to the internal field refines the exciton model.[31,32] For a quantitative understanding of this additional interaction, let us consider the dimer case discussed above. Each dimer can be modeled effectively through two states, the neutral (N) ground state, $|DA\rangle$ and the ionic (I) excited state, $|D^+A-\rangle$, with a fixed energy difference and coupling constant. For the dimer there will be four states *viz.* the neutral ground state, $|DA.DA\rangle$, two single excited states, $|DA.D^+A^-\rangle$ and $|D^+A^-.DA\rangle$ and one double excited state, $|D^+A^-.D^+A^-\rangle$. For the double excited state, due to the polarizability of the molecules, additional electrostatic interactions exist between the two $|D^+A^-\rangle$ molecules. As a result of this electrostatic interaction, the single excited state ($|D^+A^-.DA\rangle$) is stabilized/destabilized for attractive/repulsive cases respectively. Note that, the gap reduces for the head-to-tail and anti-parallel stacked arrangements of the dipoles while this increases for the other two repulsive cases. This picture is qualitatively similar to that for the exciton splitting interactions. However, within the framework of the polar-polarizable model one can quantitatively estimate the nature of stabilization/destabilization of the ground state and the excited states due to the electrostatic interactions. Since, the electrostatic interaction depends explicitly on the strengths of the Donor (D) and Acceptor (A), it is possible to predict the NLO responses of a variety of chromophores.[33]

### 2.3 H-Bonding and other weak interactions

Though dipole–dipole interactions account for a major force in the supramolecular aggregates, other important interactions include the H-bonding interactions, higher multipole interactions, weak dispersion interactions and van der Waals forces. Of these, hydrogen bonding requires special attention largely because of the unavailability of the correct potentials for such interactions within molecular mechanics (MM) framework.[34,35] Hydrogen bonding is generally considered with a geometry, D(donor)–H…A(acceptor). Some of the commonly used functions involve the modified Lennard–Jones potentials with a D-H…A angle dependent term like:[36]

$$E_{H-bond}(R) = \varepsilon\left[A\left(\frac{R_0}{R}\right)^{12} - B\left(\frac{R_0}{R}\right)^{10}\right](\cos\theta_{D-H\ldots A})^4 \quad (7)$$

where $R$ is the distance between the $D$ and $A$, $R_0$ is the equilibrium distance, $\varepsilon$ is depth of the potential and $A$ and $B$ are the adjustable parameters. The angular term ensures that the strength of the H-bonding interaction maximizes for linear D-H…A bonds.[37,38]

Popular quantum chemical methods like the density functional theory are largely insufficient to take into account long-range dispersion interactions.[39,40] Higher order wavefunction methods, like, coupled cluster calculations become very expensive for calculations on realistic NLO active molecular dimers while the MP2 level calculations are known to overbind H-bonded aggregates.[41] Apart from such problems with insufficient or too-large electron corrections, numerical calculations are also hindered due to basis set superposition error (BSSE) arising out of truncated numerical basis sets. While active research is directed towards reducing these errors, with the success of empirical methods like DFT-D (dispersion corrected)[42–44] however, *ab initio* determination of the interaction constants is still tractable. From eqn (7), the ground state of aggregates will be stabilized to the maximum extent for

 

linear D-H…A..D-H…A chains in dipolar molecules. Thus for the aggregates, H-bonding leads to an overall increase in the gap (blue shift) because the extent of charge-transfer is minimal with a very little or no excitonic splitting. Thus, H-bonding by itself is not a favorable parameter for fine tuning NLO responses in aggregates. However, a very important feature of such an interaction is that, it stabilizes linear D-H…A..D-H…A aggregates that can lead to favorable dipolar interactions with increase in the transition dipole moment.

Other than the H-bonding interactions, molecules are also stabilized through dispersion and van der Waals forces. The most prominent of such examples are the π–π stacking interactions. However, the stacking interactions provide weak ground state stability to these aggregates and in most cases, prominent dipole–dipole repulsions leads to centrosymmetric arrangement of the π-stacked chromophores and cancellation of second order NLO responses. Calculations by E. Brouyère *et al.* have concluded that for chromophores separated by distances more than 3.5 Å, "destructive π–π interactions" are prominent which lead to a reduced $\beta$ from the additive results.[45]

## 3 Modeling various molecular materials

### 3.1 Head-to-tail arrangement of paranitroaniline dimers

One of the simplest molecules possessing large NLO responses at the molecular scale is paranitroaniline (PNA) and it represents the prototype example of a Donor-π-Acceptor molecule. However, PNA molecules crystallize in a centrosymmetric point group due to strong dipolar repulsion in the parallel π-stacked dimer. However, using self-assembly techniques, it is possible to arrange molecules in head-to-tail arrangements within thin films. To obtain a quantitative understanding in general cases with high to low packed monomer densities in an aggregate, numerical calculations of the ground and excited singlet states of a dimer system have been considered. Computational work on a large aggregate is quite impossible and so one considers only double molecules. However, a dimer could provide the essential information which would be useful in predicting its behavior for a large aggregate.[46,47]

In Fig. 3(A), the variation in the optical gap with an increase in the intermolecular N–N distance between the $–NH_2$ and the $–NO_2$ for head-to-tail arrangements of the monomers is plotted. It can be clearly seen that when the molecules are far away from each other (>8 Å), the gap saturates to the monomer gap value of 4.05 eV. However, the gap reduces to 3.5 eV when the monomers are separated by a distance of 3–4 Å. Thus, if through some strategy one can stabilize the aggregate within this interchromophoric distance, it is possible to reduce the gap in an aggregate. Geometry optimization of the dimer leads to the formation of a head-to-tail arrangement with two N–H…O H-bonding interactions which stabilize this specific dimer with a N…N distance of 3.4 Å. Thus, specific H-bonding interactions will create "tailor-made" situations for favorable excitionic splitting interactions. Further calculations on the stabilization energy of the dimer at MP2/6-31+G (d,p) level (considering counterpoise correction to remove basis set superposition error and zero-point vibrational energy correction)[48,49] shows that this arrangement is stabilized by $\approx$ 10 kcal mol$^{-1}$, which is quite substantial to provide stability in a supramolecular assembly (Fig. 3(C)).

Calculation of the optical gap and the second harmonic coefficients requires an accurate determination of the excited states and oscillator strengths for these states. This can be done

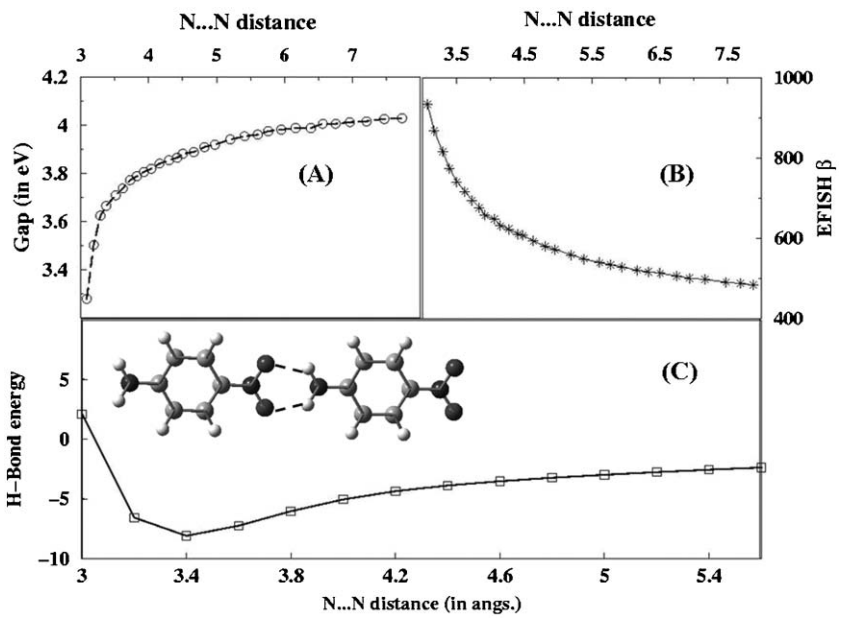


**Fig. 3** (A) Lower optical gap (in eV) with increase in intermolecular N…N distance (in Å) between the $–NH_2$ and $–NO_2$ for the head-to-tail arrangement of PNA molecules. (B) Electric field induced second harmonic generation (EFISH) coefficient (in esu units) as a function of N…N distance (in Å). (C) Potential energy profile for the H-bonding interactions in the PNA dimer (in kcal mol$^{-1}$) (molecular structure shown is for the minimum energy structure).

within substantial reliability through semi-empirical methods like ZINDO/MRDCI (multi-reference doubles configuration interaction) formalism with correction vector (CV),[50–56] the Finite-Field methods[57–59] including non-local correlations within DFT formalism[60] and also through the time-dependent DFT methods[61] which have been gaining popularity in recent times. For linear and 1-D systems, the SHG coefficient ($\beta$) is essentially along the long polarization axis. However, for most systems, one needs to consider polarizations for the material along all the axes and define a tumbling average $\beta_{av}$ = 1/3 ($\beta_{xyy}$ + $\beta_{yyx}$ + $\beta_{yxy}$)

The fact that the gap can be reduced through excitonic splitting by favorable intermolecular interactions allows one to fine tune the NLO properties of an aggregate. This is seen in the NLO response of the dimer with an increase in the N…N distance (Fig. 3(B)). One can qualitatively understand this on the basis of the two-level model. $\beta$ within a two-level model, can be written as[62]

$$\beta_{\text{two-level}} = \frac{3e^2}{2\hbar}\frac{\omega_{12} f \Delta\mu_{12}}{\left(\omega_{12}^2-\omega^2\right)\left(\omega_{12}^2-4\omega^2\right)} \quad (8)$$

where $\hbar\omega_{12}$ is the excitation energy, $f$ the oscillator strength, $\Delta\mu_{12}$ the difference between the dipole moments of the ground and the excited state and $\omega$ specifies the excitation frequency of the oscillating electric field. The most important factor in the above simple expression is that the SHG coefficient is directly proportional to the oscillator strength and the dipole moment difference. These two quantities are naturally high in the head-to-tail arrangements. For a favorable arrangement as discussed earlier, we also note that the exciton level energies to the lowest dipole allowed state reduce, which in the expression above appears in the denominator as a result of which the SHG coefficient would increase.[63]

The excitonic gap reduces while oscillator strength and $\mu\beta$ increase dramatically at small N…N distances where hydrogen bondings are possible. Although excitonic splitting is proportional to only $4\mu^2/r^3$ in this case, due to hydrogen bonding, the $\mu\beta$ value is almost 14 times greater than the monomeric $\mu\beta$. Considering the two-level $\beta$ value, which is proportional to both $\Delta\mu$ and $f$, the Frenkel exciton estimate would give $\mu\beta$ $\sim$ 380 esu at small distances. At large distances of course, the $\mu\beta$ value is what is expected from exciton theory.

The configuration in Fig. 3(C) is an asymmetric dimer. The exciton theory based on dipole–dipole interactions provide a small shift in the adsorption spectra ($\sim$0.011 au) even at small distances, with oscillator strength of the order 0.4. The strong red-shift at small distances is mainly due to hydrogen bonding. The lowest singlet excited state in the dimer is excitonic in character. These excitations possess appreciable intensity and are associated with an appreciable dipole moment change, along the long axis of the dimer. The calculated low-energy excitonic character can be associated with the long-wavelength features observed in J-band aggregates.[64,65] Coupled with the discussion above, one can thus safely conjecture that the PNA aggregates with hydrogen-bonded chromophores lying *in-line* can give rise to a large $\beta$ value, with a one-photon absorption frequency deep inside the IR-region. A few experimental confirmatory examples of such planar (although not exactly *in-line*) monomeric stacks, with large SHG coefficients have been reported.[66,67]

### 3.2 Quantitative comparison of the role of dipolar interactions and H-bonding interactions

While, dipole–dipole interactions have effects on NLO properties of aggregates through excitonic splitting as discussed for the previous case, the role of H-bonding governing the NLO properties in head-to-tail arrangements are rarely investigated in detail. The strength of the hydrogen bonding is generally understood on the basis of its partition into various contributions like the electrostatic energy, exchange repulsion energy, polarization energy and charge-transfer energy.[68] Out of these terms, the charge-transfer(CT) effects are very important in controlling the NLO responses as they increase the transition dipole moment from the ground state to the optically active states. The CT salts are well-known to possess large off-resonance NLO properties.[69] Although, the charge-transfer efficiency in hydrogen bonding is quite small, it should depend on many factors including the strength of H-bonds. In fact, as mentioned in the Introduction, the contribution of H-bonding to the collective NLO responses in aggregates seems to be ambiguous. So, a proper understanding can be gathered through the systematic variation in the strengths of H-bonding.

To critically examine the effects of H-bonding on second order polarizabilities ($\beta$), we considered a series of 1-D assemblies connected through H-bonding. The model system considered is a linear HX (X = F, Cl, Br) chain. HX provides a nice variation of the strength of bonding between the molecules (HF > HCl > HBr). While the HF chain has the strongest H-bonding, interactions in HBr chains is seemingly dispersive and the interactions are more dipolar in nature. Additionally, we also consider pure dipolar aggregates such as a linear CO chain for a quantitative comparison and contrast.

The bond lengths for HF, HCl and HBr are calculated as 0.950 Å, 1.28093 Å and 1.42354 Å at B3LYP/aug-cc-pVQZ level. The distance between each HX monomer is kept constant for all chain lengths ($d$ = 1.87 Å for HF, $d$ = 2.665 Å for HCl and $d$ = 3.178 Å for HBr). Fig. 4 shows the linear chains considered with the H–X…H distances. These are the standard average distances that are found from calculations of the geometry optimized structures of the linear chains.

For an analysis of the energetics associated with these structures, the binding energies for the clusters are calculated

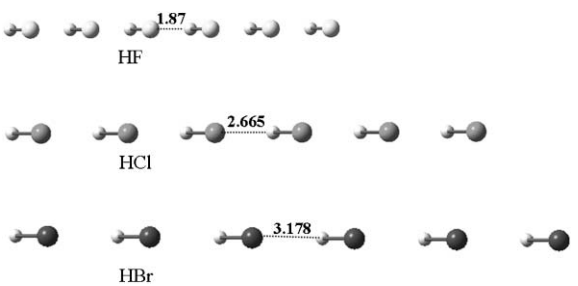


**Fig. 4** Structures for the linear chains of HF, HCl and HBr. The distances (in Å) between each monomer is kept constant as shown in the figure.

 

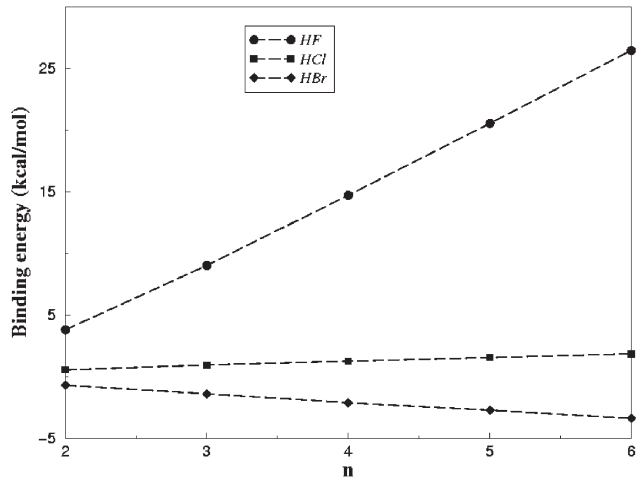


**Fig. 5** Variation of binding energy, $\Delta E$ for different sizes of clusters for HF, HCl and HBr in linear chains. The reported energies include corrections for BSSE and ZPVE (see text).

using the definition: $\Delta E_{0,n} = nE_0\,[(\mathrm{HX})] - E_0\,[(\mathrm{HX})_n]$. All the energies are corrected for zero-point vibrational energy (ZPVE) corrections and the basis set superposition errors (BSSE). BSSE are calculated using the counterpoise correction(CP) scheme and the reported results incorporate the CP corrections. Fig. 5 shows the binding energies in HF, HCl and HBr at the MP2/6-311++G(d,p) level (for cluster sizes upto $n = 6$). The binding energies for the HF chain increases with an increase in the cluster size. However, the binding energy remains almost constant for the HCl chain and for the HBr chain, the binding energy decreases with an increase in the chain length. The negative binding energies for the HBr clusters arise essentially due to the fact that the stable clusters of the $(HBr)_n$ are cyclic and the linear chains are the high energy structures. However, the linear HBr chains act as a model to mimic the H-bonding in the weak interactions limits for chromophores arranged in a 1-D manner. It is thus interesting to examine the non-linear optical properties for the 3 limiting cases of stability in these chains.

The 1st hyperpolarizabilities ($\beta$) for the three cases show entirely different pictures (seen from Fig. 6). For the $(HF)_n$, $\beta$ increases initially till $n = 3$ and then decreases. As already mentioned, there is a very strong H-bonding and such local maxima show a clear signature of H-bonding effects. For HCl and HBr however, there are no signs of decrease in $\beta$ with increase in the chain length. The HCl chain shows a sharp increase till $n = 3$ and then increases slowly. A rapid increase implies that H-bonding is still active for HCl at smaller oligomeric length but unlike HF, the bonding is not stronger enough to reduce $\beta$ with an increase in $n$. For HBr however, there is a uniform increase in $\beta$ with the increase in chain length and the profile shows no discontinuity indicating that H-bonding is very weak for all values of $n$ and does not lead any special polarization effects.

For a clear comparison of these H-bonded systems with a purely dipolar aggregate, the NLO coefficients of a linear CO chain are also calculated. The distance between each CO unit in the linear chain is found to be 3.95 Å, while the CO bond-length is 1.13 Å. The large CO…CO distance indicates pure dipole–dipole interactions. This CO linear chain mimics interactions in many NLO crystals constituted of π-conjugated molecules like PNA and MNA without however the H-bonded interactions. Thus, an analysis based on only a dipolar aggregate allows one to understand the effects of the dipolar component in a more detailed manner. For the CO chain, $\beta$ has a linear behavior with an increase in the nuclearity. Thus, when there are no effects of H-bonding, $\beta$ has a linear profile. The deviation from the dipolar interactions increase in the

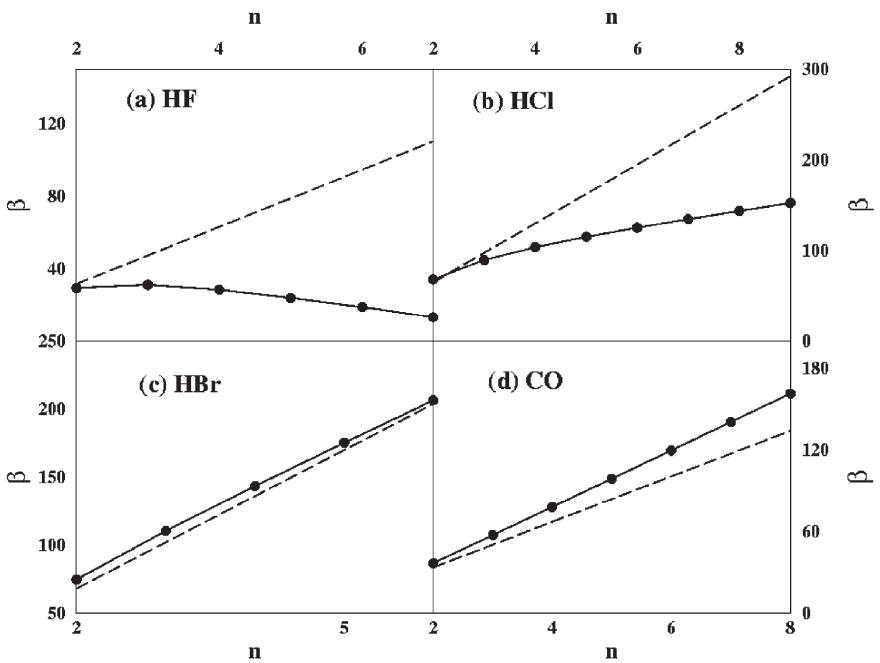


**Fig. 6** Variation of $\beta_n$ (solid line, with circles) and $n\beta_1$ (dotted line) for HF, HCl, HBr and CO. Note the close similarity in profiles for HBr and CO.

order HBr < HCl < HF. In the limiting cases of weak H-bonding, the 1st hyperpolarizability is mainly governed by the dipolar interactions. However, the decrease of $\beta$ with increase in $n$ must have an H-bonded origin which shows large cooperative phenomena of decreasing $\beta$ with increasing $n$. It is interesting to note that the interactions with various length scales can lead to completely different NLO features.

For a quantitative understanding of the cooperative nature of various interactions, we compare the $\beta$ of a molecular chain $\beta_n$, with $n$ isolated molecules, $n\beta_1$ (where $\beta_1$ is the SHG of a single monomer). These two quantities are plotted in Fig. 6 for all the four systems. HF shows a highly non-linear profile in $\beta_n$ with large deviation from the linear multiples of monomers ($n\beta_1$). The polarization of the whole system decreases with strong H-bonding between the monomers. HCl also shows a deviation wherein the $\beta_n$ increases with the increase in $n$ but the increase is slow, however, with a positive slope. The cases for HBr and CO are very similar. For both of them, $\beta_n$ has a larger value than $n\beta_1$ implying that the contribution of dipole–dipole interactions (Davydov splitting) towards polarizations helps increase $\beta_n$, in contrast to ''strong'' H-bonding. Thus, cooperative damping in the NLO properties decrease with a decrease in the strength of H-bonding for linear 1-D aggregates.

The reduction in the magnitude of $\beta_n$ with an increase in $n$ for HF can be traced to the change in the polarizations of the ground state in comparison to the dipole allowed excited state. We find that for the HF chains, there is a large increase in $\Delta\mu(\mu_{ex} - \mu_{gs})$ at small chain lengths ($n$ = 2), but a steady decrease in its magnitude with the increase in the chain length. For CO however, the $\Delta\mu$ increases with an increase in chain length. From the two-level expression for $\beta$, an increase in the magnitude of $\Delta\mu$ implies large $\beta$. This explains the initial increase of $\beta$ for HF at small chain length (cooperative phenomena) and the monotonic increase of $\beta$ for CO, with an increase in $n$. For the weaker H-bonded systems like HCl and HBr, the $\Delta\mu$ profiles progressively become similar to the purely dipolar CO profiles.

To further understand the reason behind such a large polarization at small chain lengths for the strongly H-bonded systems, the Mulliken charge densities on the electronegative F-atom are calculated with the increase in the chain length, both in the ground and the lowest optically excited state. In the ground state (GS), $\delta^-_F \approx -0.5$ for all chain lengths. In the excited state (ES), however, only for the monomer (H–F) is there a strong feature of change in polarity (increased ionicity). For example, for HF ($n$ = 1), $\delta^-_F$ (ES) $\approx$ +0.316. But as $n$ increases, the average ionicity decreases. Thus, for $n$ = 2 only one of the F atoms is ionic and the other F atom remains at $\delta^-_F \approx -0.5$ similar to that in the GS. With further increase in $n$, the ionic contribution decreases further. Since for every $n$, there is only one F atom which is polarized in the excited state, the reduction in average ionicity with increase in $n$ is of the order $\sim 1/n$. Note that the F atom which is polarized in the excited state is involved in hydrogen bonding with the neighboring H atom while its own hydrogen partner remains at the chain end without H-bonding. Interestingly, out of three types of F atoms in the $(HF)_n$ chain, the leftmost H–F is different and so is polarized. This is purely due to the chain nature of the aggregates and explains the decrease in $\Delta\mu$ as well as the $\beta$ with the increase in $n$ for HF. Thus, the boundary conditions play a very important role in determining the local polarizations in an aggregate. CO, on the other hand, is predominantly covalent and thus the ionic contribution in the ES is small. $\delta^-_O$ is $\approx -0.29$ both in the GS and the ES and no local polarization effects are found. On the application of an electric field, all the $\pi$-electrons in the $(CO)_n$ are polarized, resulting in an increase of $\beta$ with an increase in $n$.

The computations based on linear and quasi one-dimensional chains serve as a rule of thumb model for estimation of interactions in actual crystalline geometries for most NLO active H-bonded compounds. It is favorable to have H-bonding in the intermediate regime [between (HCl…HCl) and (HBr…HBr) limits] for large NLO coefficients across 1-D chains. As has been seen earlier, very strong H-bonding as that for HF…HF reduces the NLO response functions.[70] Although there is an enhancement of $\beta$ even for pure dipolar aggregates like CO…CO, such chains are not stable and the linear directionality of the aggregate is not maintained. The same is true for the very weakly H-bonded HBr…HBr. This is interesting, because, in most crystals as well as in biological systems like DNA and proteins, H-bonding in the intermediate energy scales like N–H…O, N–H…N, O–H…O *etc.* are most predominant. Thus, a relatively weak H-bond creates a balance between the actual stability of the aggregate and an increase in the NLO response functions.

### 3.3 Oxygen bridged double molecule: PNA–O–PNA

Apart from the utilization of weak intermolecular forces like H-bonding and $\pi$-stacking interactions, D-$\pi$-A molecules can be arranged in desired orientations through specific functional groups. For example, two PNA molecules can be arranged in side-by-side fashion in a non-centrosymmetric fashion through connectivity in the *ortho*-position by an oxygen atom. Similar compounds have been synthesized.[71,72] The ground state optimized structure for such a molecule is shown in Fig. 7(A). Due to the $sp^3$ hybridized nature of the bridged O-atom, the two PNA molecules are orientated in two different planes with the interdipolar angle ($\phi$) which is calculated as 43.4° at the AM1 (Austin Model 1) level. Frontier orbital analysis shows that there is almost no overlap within the $\pi$-electrons of the two PNA rings.[73] The optimized structure for two PNA molecules bridged by the C–C linkage in the *meta*-position is shown in Fig. 7(B).

Fixing one PNA molecule and rotating the other PNA molecule along the O–PNA axis changes the interdipolar angle ($\phi$) from 0 to 180°. The conformation for $\phi$ = 0° corresponds to the parallel side-by-side arrangement of the dipoles while $\phi$ = 180° corresponds to the anti-parallel arrangement. Thus, it is interesting to ask what happens to the second harmonic response of the molecular dimer as one changes the interdipolar angle. Molecules with different interdipolar angles can be synthesized by suitable substitution of alkyl groups on the rings that can stabilize specific orientations of $\phi$.

In Fig. 8 (Upper panel), the total ground state dipole moment $\mu_G$ (in Debye) for PNA–O–PNA is plotted against variation in the interdipolar angle. The dipole moment decreases with an increase in the interdipolar angle. This can

 

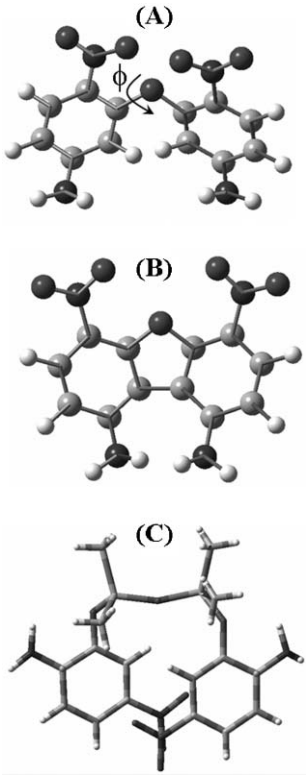


**Fig. 7** (A) Ground state optimized structure of PNA–O–PNA at the AM1-level. $\phi$ represents the interdipolar angle. (B) Optimized structure of PNA–O–PNA bridged through the C–C linkage at the *meta*-position. (C) Molecular structure of PNA–O–Si$(CH_3)_2$–O–Si$(CH_3)_2$–O–PNA as retrieved from the Cambridge Crystallographic Database (CCDC).

easily be understood by considering the combined effects of ground state dipoles of each monomer. If the two dipoles are parallel and in the same plane, the *in-phase* combination ($\phi$ = 0°) of the resultant dipole is the sum of the two individual dipoles.

The bridged oxygen atom does not play any significant role in determining the non-linear optical coefficients. It basically controls the distance between the two nitroaniline dipoles. Due to its high electronegativity, it just increases the total dipole moment of the dimeric systems (it is roughly 1 Debye increase purely because of oxygen) to the same extent for all values of the dihedral angle, $\phi$. The minimum distance between the dipolar axes of the molecules is more than 4 Å, thereby, ensuring that no explicit intermixing of the π molecular orbitals of the chromophores which validates the exciton theory discussed earlier based on the dipole–dipole interaction model. Thus, even though the semi-classical theory of dipole–dipole interaction does not take into account the electronic properties of the bridged O atom, it is found that the qualitative trend in splitting energy as a function of the angle, $\theta$, is almost the same with those obtained from single-configuration interactions (SCI) calculations for the di-nitroaniline systems.

For the calculations of the optical coefficients, an excitation frequency of 1064 nm (1.17 eV) which corresponds to the frequency of the Nd–YAG lasers is used. The variation in EFISH (electric field induced second harmonic coefficients) coefficients with the increase in the dihedral angle ($\phi$) is shown in Fig. 8(Lower panel). The trend is very similar to that for the ground state dipole moment in Fig. 8(Upper panel). To be precise, the magnitude of the EFISH coefficient decreases with an increase in the torsional angle for the PNA–O–PNA.

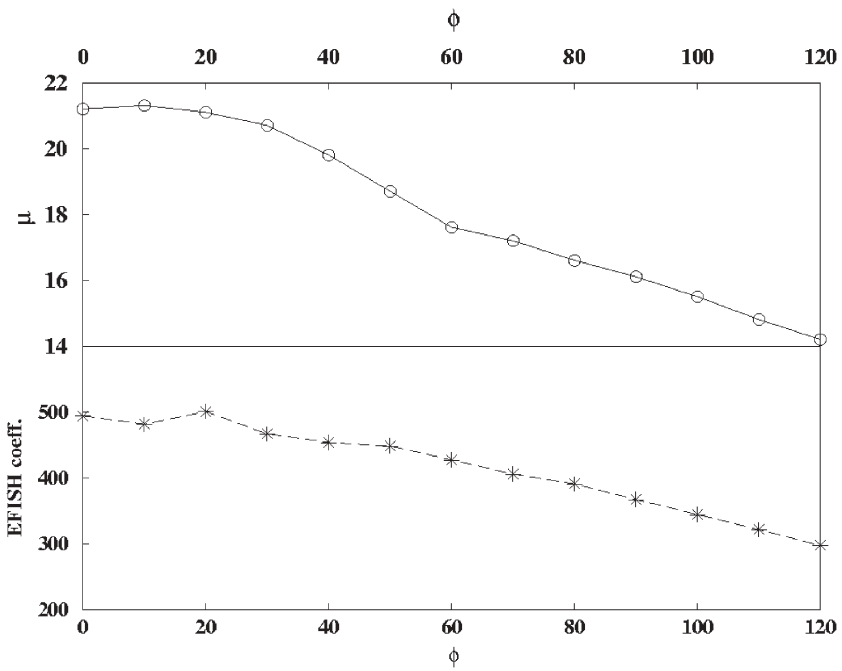


**Fig. 8** (Upper panel) Variation of the ground state dipole moment ($\mu$) (in Debye) with an increase in the interdipolar angle (in degrees). (Lower panel) Variation of the EFISH coefficient ($\mu\beta$) (in esu units) with an increase in the interdipolar angle (in degrees).

The results compare fairly well with the experimental values. For example, the calculated $\beta$ for the optimized geometry *bis (2-amino-4-nitrophenyl) ether* ($\phi$ = 43°) is $\beta$ = 16.4 × $10^{-30}$ esu,[71] while the experimental value for the Hyper-Rayleigh Scattering (HRS) experiments at the Nd:YAG frequency is 22.0 × $10^{-30}$ esu.

A very important aspect of the above discussion is to design the di-nitroaniline system so that the maximum NLO activity can be attained. The highest EFISH coefficients (494.4 × $10^{-30}$ esu) are obtained for the PNA–O–PNA with zero dihedral angle. Such a high value of EFISH coefficient is not possible to realize from real molecular systems as the optimized geometries of the di-nitroaniline molecules discussed above are not planar due to steric repulsions. Therefore, the best suggestion is to connect the oxo-bridged rings by a carbon–carbon bond in the *meta*-position. Optimizations of this structure, (shown in Fig. 7(B)) at the AM1 level of theory, confirms that the nitroaniline rings are almost planar with the dihedral angle $\phi$ very close to zero. Thus one can make the two dipoles to be parallel to a large extent by bridging the two rings by a covalent bond. The EFISH coefficients for this bridged structure is 471.5 × $10^{-30}$ esu, which is close to the parallel ($\phi$ = 0) PNA–O–PNA dipole value.[73]

To further verify the existence of such bridged dimers of PNA–O–PNA, a detailed search for such structures in the Cambridge Crystallographic Database was performed. A very interesting structure, similar to our theoretically considered structure is that for PNA–O–Si$(CH_3)_2$–O–Si$(CH_3)_2$–O–PNA (CSD id: TOFPIN.cif) (see Fig. 7(C)).[72] The monomers are connected by a siloxane bridge. The presence of such siloxane backbones provides large thermal stability and mechanical strength to the dimer. Being rigid, this backbone locks the two monomers in non-centrosymmetric orientations with an interdipolar angle of 36°.

### 3.4 Parallel and frustrated arrangement of dipoles in calix[3]arenes

Much efforts have been directed towards the synthesis of calix[n]arenes in the last decade.[74–76] In this class of systems, the individual chromophores are arranged in the form of 'baskets' by connecting the constituent molecules by linkers like $(CH_2)_n$ or $(CH_2O)_n$. Thus, these compounds provide an innovative way to arrange the chromophores in a parallel arrangement.[77] Moreover, one can even increase the number of chromophores in such an assembly by changing '*n*'. The interdipolar angle can be varied by functionalizing the lower and upper rims of the 'baskets' with groups of different sizes. The overall structure is then controlled by steric classes of interactions. It would thus be very interesting to understand the mechanism of interactions of the individual dipoles of the chromophores in such a multi-molecular assembly and how such forces control the overall NLO properties of the calix[n]arenes. In fact there have been quite a large number of efforts to theoretically understand NLO effects in such confined geometries of calix[n]arenes.[45,78–80]

The NLO properties in calix[3]arenes can be modeled through similar geometrical arrangements in hydrogen fluoride trimer, $(HF)_3$. The dipole interactions in such a model

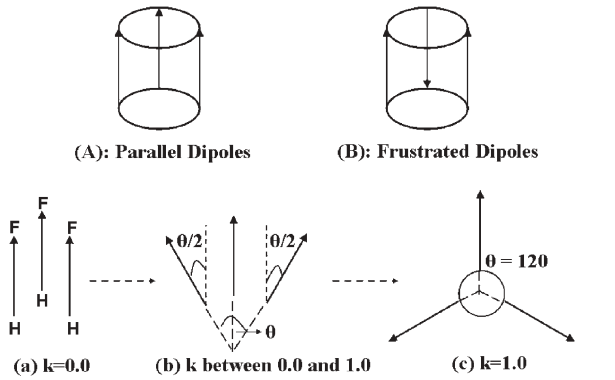


**Fig. 9** Arrangement of dipoles in a basket-type geometry for (A) parallel and (B) anti-parallel geometries. (a) Parallel dipoles with interdipolar angle, $\theta$ = 0°. (b) Geometry as the dipoles open up, the lower rim radius remains constant and the upper rim radius changes. (c) Fully opened basket with interdipolar angle, $\theta$ = 120°.

can be varied by: (i) Changing the inter-dipolar angle. This amounts to an opening up of the 'baskets'. (ii) Increasing the inter-dipolar distance. The arrangement is shown in Fig. 9. Three HF molecules are arranged parallel to each other so that the lower base (lower rim) has three H atoms and the upper base (upper rim) has three F atoms. The three H and the three F atoms in each rim form two equilateral triangles. This is the all-parallel arrangement for the dipoles, applicable for a parallel cylindrical arrangement as in calix[n]arenes.

However, the most stable arrangement of such a dipolar arrangement is the anti-parallel arrangement. Systems like calix[3]arene have a significant percentage of the anti-parallel form (u,d,u; u,u,d) apart from the all-parallel cone geometry (u,u,u or d,d,d).[81] A complete relaxation from the all-parallel to the anti-parallel arrangement is possible only for calix[n] arenes with even numbers of chromophores, $n$ = 4,6,8 *etc.* For odd numbers of dipoles in the assembly, such a relaxation is, however, not possible resulting in the formation of a frustrated orientation. For example, for $n$ = 3,5,7 *etc.* the dipoles are in a *frustrated* arrangement, where, the overall dipole-moment for the relaxed geometry does not vanish. The individual chromophores in calix[n]arenes are connected by short bridges that prevent random orientations of the dipoles. In fact, the $(HF)_3$ system is the simplest case for a molecular assembly that can be studied for both parallel and frustrated cases simultaneously. For such a 'frustrated' arrangement with the basket opening up, a favorable hydrogen-bonding interaction is developed, which further stabilizes the system. It is interesting to note that dipolar frustration is quite different from frustration in magnetic materials. The parallel case of dipoles in Fig. 9(A) corresponds to repulsive interactions while for a magnetic system, parallel orientation of spins will lead to a ferromagnetic ordering. Similarly, the frustrated orientation of dipoles in Fig. 9(B) leads to an attractive interaction with a net dipole while for magnetic systems, such orientations of spins lead to highly degenerate classical ground states with net spin moment equal to zero.

The inter-dipolar angle for real molecular systems is controlled by the steric bulk of the groups on the lower and the upper rim of the cylinder. Increasing the bulkiness of the

 

groups in the upper rim while keeping the steric bulk of the lower rim constant, increases the inter-dipolar angle, with an opening up of the basket. Thus, the system having a cylindrical symmetry is converted into a conical-shaped geometry.

For modeling the opening up of the cylinder for both the parallel (seen in Fig. 9(A)) and frustrated dipoles (seen in Fig. 9(B)), the lower rim corresponds to three atoms whose coordinates are kept constant and the coordinates of the three atoms in the upper rim is varied. The radius of the upper rim can be increased by translating the corresponding atomic coordinates according to: X = X + $k$X, Y = Y + $k$Y and Z = Z − $k$Z, while keeping all the three molecular (HF) bond lengths fixed. The Z-axis corresponds to the internuclear axis and $k$ is the flattening parameter which varies from 0 to 1.0. While the $k$ = 0 case corresponds to the perfect cylindrical arrangement for an inter-dipolar angle $\theta$ = 0°, the $k$ = 1.0 signifies the other extreme where the cylinder becomes completely flat (Z coordinates are zero) so that all the six atoms (3H and 3F) are on the same plane, forming a circular disk. For such a case ($k$ = 1.0), the inter-dipolar angle $\theta$ = 120°. For all intermediate values of $k$, between 0.0 and 1.0, the cylinder is progressively opened and the inter-dipolar angle, $\theta$, increases from 0° to 120°.

With the dipoles opening up, the total ground state dipole moment changes as a function of the inter-dipolar angle. A general dipole moment expression for the combined effect of three dipoles can be written as

$$\mu_G = \sqrt{\mu_a^2 + \mu_b^2 + \mu_c^2 \pm 2\mu_a\mu_b\cos\theta_{ab} \pm 2\mu_b\mu_c\cos\theta_{bc} \pm 2\mu_c\mu_a\cos\theta_{ca}} \quad (9)$$

where $\mu_a$, $\mu_b$ and $\mu_c$ are the dipole moment vectors for three dipoles $a$, $b$, $c$ and $\theta_{ab}$, $\theta_{bc}$ and $\theta_{ca}$ represent the angles between the corresponding dipoles. Note that the dipolar angle determines the phase (+ve for parallel and −ve for frustrated arrangement) of the dipoles.

For the present case when all the dipoles are the same (homomolecular system), $\mu_a = \mu_b = \mu_c = \mu_i$ and $\theta_{ab} = \theta_{bc} = \theta_{ca} = \theta_{ij}$. In the parallel orientation, all the vectors are in-phase. Thus, the total dipole moment is given by

$$\mu_G = \sqrt{3\mu_i^2 + 6\mu_i^2\cos\theta_{ij}} \quad (10)$$

For $\theta_{ij}$ = 0°, the $\mu_G$ has a maximum value of $3\mu_i$. When $\theta_{ij}$ increases from 0° to 120°, the $\mu_G$ decreases monotonically to zero.

In the frustrated arrangement, two of the inter-dipolar angles are out-of-phase and one of them is in-phase. Thus the total dipole moment is

$$\mu_G = \sqrt{3\mu_i^2 - 2\mu_i^2\cos\theta_{ij}} \quad (11)$$

For this geometry, the $\mu_G$ increases from $\mu_i$ (for $\theta_{ij}$ = 0°) to $2\mu_i$ (for $\theta_{ij}$ = 120°). Thus, for such a frustrated dipolar system, the ground state dipole moment is a monotonically increasing function of the inter-dipolar angle.

The above expressions for the dipole moments are purely classical without any correlation among the dipoles. However, for systems with non-zero ground state dipole moments, there exists a strong dipole–dipole interaction. Such interactions lead to a large excitonic coupling and the effects are most prominent in the excited states of the molecules. For such aggregates, while the ground state is stabilized with respect to the monomers, the excited states which remain degenerate at infinite distance between the monomers, undergo splitting into three states, ($E_1$, $E_2$ and $E_3$), when they are brought closer. Interestingly out of the these three, two ($E_1$ and $E_2$) will be degenerate while $E_3$ is non-degenerate and symmetric. The extent of splitting, $\Delta E$, will, of course, depend on the strength of dipole–dipole interactions.

With the increase in the inter-monomer angle corresponding to the flattening up of the basket, there is a variation in the oscillator strength in the three states, $E_1$, $E_2$ and $E_3$. For the parallel case, at $\theta$ = 0, $E_3$ only is the dipole allowed state with large oscillator strength since it is associated with the *in-phase* combination of the three dipoles. However, as the interdipolar angle increases, in addition to $E_3$, $E_1$ and $E_2$ also become dipole allowed, more so for large flattening. For the frustrated assembly, however, all the states are dipole allowed at $\theta$ = 0 and as $\theta$ increases, the $E_1$ and $E_2$ become strongly allowed (higher oscillator strength) while $E_3$ becomes progressively weaker.

The variation of the dipole moment with the inter-dipolar angle for the all-parallel geometry of the dipoles is plotted in Fig. 10. The inter-dipolar distances ($d$) are varied from 1.5 Å to 4.5 Å. For comparison, in the same plot, the results as derived from the analytical classical dipole moments (shown in eqn 10) are also plotted.

At small interdipolar distances like 1.5 Å, the computed dipole moment shows a very large deviation from the non-interacting analytical value. For example, at $\theta$ = 0°, the magnitude of the total dipole moment is only 3.97 Debye compared to the classical value of 5.42 Debye, a reduction of 27%. But, as the basket opens up, the deviation decreases and both the computed and the analytical values converge to 0 Debye for $\theta$ = 120°. This signifies the role of electronic

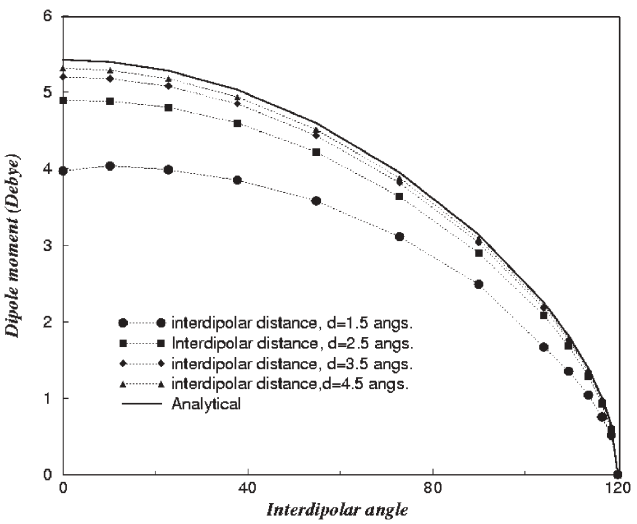


**Fig. 10** Ground state dipole moment, as a function of the inter-dipolar angle, $\theta$, for the parallel dipolar assembly.

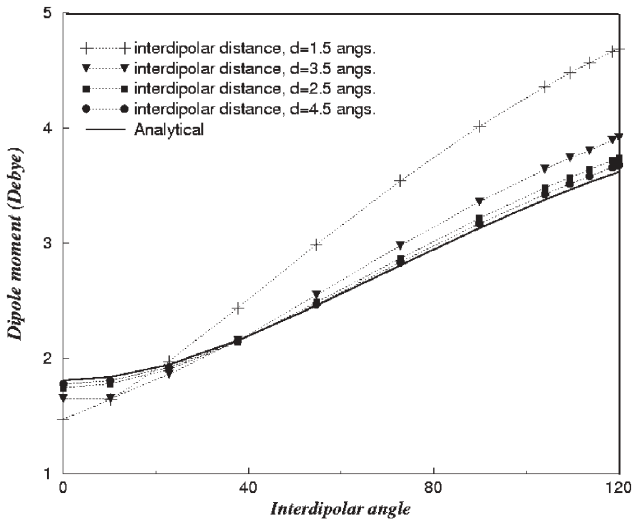


**Fig. 11** Ground state dipole moment, as a function of the inter-dipolar angle, $\theta$, for the frustrated dipolar assembly.

correlations for the $(HF)_3$ assembly at small inter-dipolar distances and small inter-dipolar angles. But, as the inter-dipolar distance ($d$) between the HF monomers increases around ($d \sim 4.5$ Å), the intermolecular interactions decrease and the system transforms into a classical dipolar assembly, so that the classical expression for the dipole moment ($q.r$) remains valid at large interdipolar distances.

The variation of $\mu_G$ for the frustrated dipolar system shows very interesting features (see Fig. 11). At small inter-dipolar angles, the calculated dipole moments differ from the classical values particularly at small $d$. This is similar to the case for parallel dipoles. However, contrary to the parallel dipoles (see Fig. 10) where, with increase in the dipolar angle, the deviation becomes less prominent, the frustrated dipolar systems show very large deviation from the classical dipole moment values for large $\theta$. The deviation is the largest for the case of small inter-dipolar distances of d = 1.5 Å.

As the basket starts to open up, two of the hydrogen atoms in two HF molecules come close to the fluorine atom of the third HF molecule. Initially the F…H–F angle is 90° but as the dipoles flatten up, the F…H–F angle increases towards 180°. Such a linear F…H–F conformation has been found to be most suitable for the H-bonding interaction. Therefore, with the increase in the inter-dipolar angle, the H-bonding interaction increases for the frustrated cases. The effect is most profound for the small inter-dipolar distances of 1.5 Å as the F…H–F bond is strongest at such distances. H-bonding interaction being primarily electrostatic in nature, not only the linearity, the distance between the electronegative atom and hydrogen atom also is crucial for effective charge transfer. Therefore, there is an overall enhancement of 30% in the dipole moment magnitude compared to the non-interacting value in the ground state dipole moment at small inter-dipolar distances and large $\theta$ values. However, as the inter-dipolar distance increases, the H–F…H bond becomes weaker and there is very little enhancement in the dipole moment from the classical value.

In Fig. 12, the first hyperpolarizability ($\beta$) is plotted as a function of the inter-dipolar angle and the distances between them for the parallel orientations. At a small inter-dipolar distance of 1.5 Å, the magnitude of $\beta$ decreases very rapidly with the increase in the inter-dipolar angle till $\theta \approx 30°$ (Fig. 12(a)). After such an initial steep decay, $\beta$ decreases monotonically and reduces to zero at $\theta = 120$.

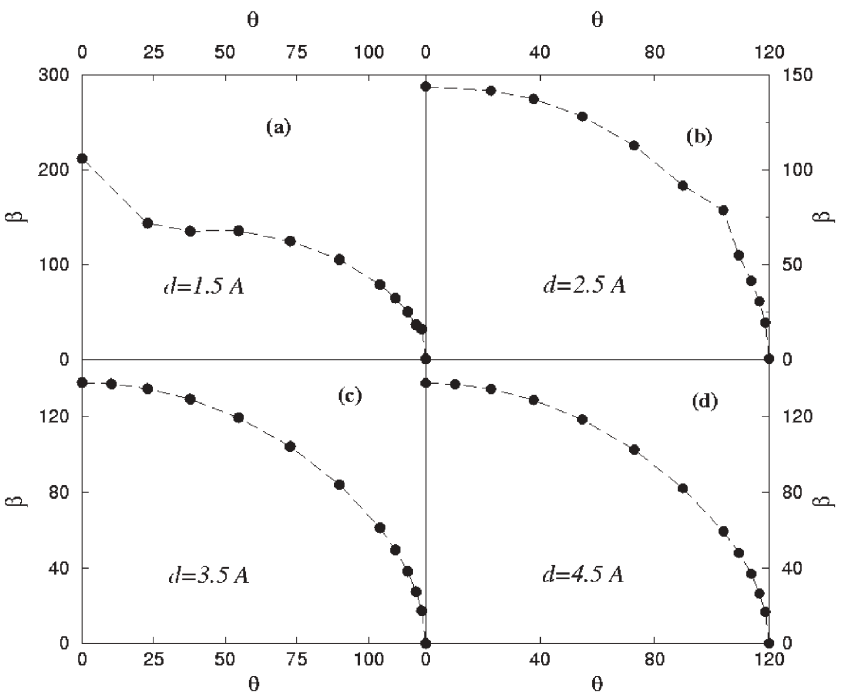


**Fig. 12** Variation of $\beta$ with respect to the interdipolar angle at varying interdipolar distances ($d$), for parallel orientation at TDHF/6-31G(d,p) level. $\beta$ is in atomic units.

 

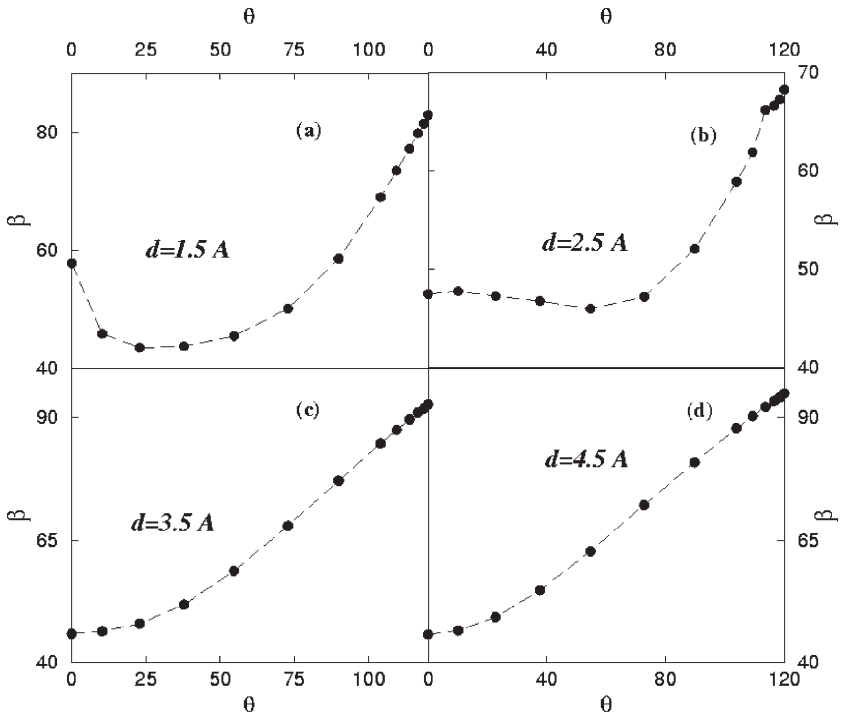


**Fig. 13** Variation of $\beta$ with respect to the interdipolar angle at varying interdipolar distances ($d$), for frustrated orientation TDHF/6-31G(d,p) level. $\beta$ is in atomic units.

The frustrated dipolar assembly (case B in Fig. 9) also exhibits very similar qualitative trends. For a small inter-dipolar distance of 1.5 Å, $\beta$ decays with the increase in the inter-dipolar angle till $\theta \approx 30^\circ$ (Fig. 13(a)). At larger inter-dipolar distances, $d$ = 2.5 Å (Fig. 13(b)), 3.5 Å (Fig. 13(c)) and 4.5 Å (Fig. 13(d)), where the optical gap saturates, $\beta$ shows a monotonic increase with the increase in the interdipolar angle.

Fig. 14 shows the structures of the two calix[3]arenes for which the NLO calculations are performed. The structures are optimized at the *ab initio* level using the B3LYP method at a 6-31G++(d,p) basis set. The geometry optimized synthon, $(CH_3)_3C–Ph–NO_2$, is also shown. Selection of this monomer is ideal, because, the steric interaction between the *tert*-butyl groups will prevent the aggregate to flatten. Additionally, three synthons are connected by $–CH_2–CH_2–CH_2–$ units. Thus the change in the optical properties in the aggregate and the individual monomer can be understood on the basis of the model $(HF)_3$ confined within the calix[3]arene geometry, as discussed above.

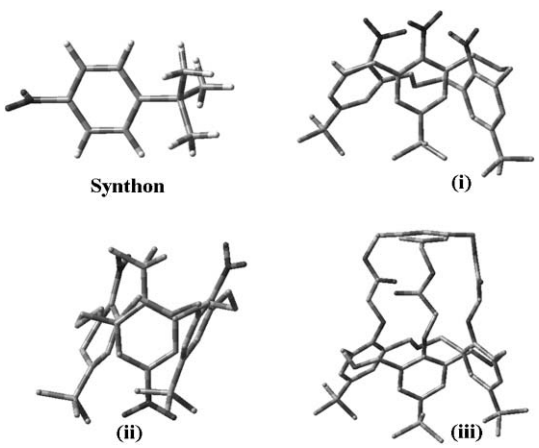


**Fig. 14** Structure of the synthon, $(CH_3)_3–Ph–NO_2$: (i), the all-parallel dipolar aggregate; (ii), the frustrated dipolar aggregate; (iii), geometry from crystal structure of a molecule in all-parallel arrangement of dipoles. H not displayed in (i), (ii) and (iii) for clarity.

Dipoles are arranged in parallel orientations as shown in Fig. 14(i). However, as can be seen from the structure, the monomers do not make the same phase angle with each other as the structure relaxes from the exact parallel arrangement to a relaxed geometry. For the molecule shown in Fig. 14(ii), a similar case of frustrated dipolar geometry as that in $(HF)_3$ case is considered. Two of the $(CH_3)_3C–Ph–NO_2$ moieties are parallel while the third one remains anti-parallel to the other two. Energy minimization for the structure leads to a relaxation from the unidirectional orientation. The dipole moment of the monomer is 5.92 D while the aggregate (i) has a dipole moment of 13.1 D. One can calculate the average cone angle, $\theta_{ij}$, for such an arrangement using eqn (10), since $\mu_G$ and $\mu_i$ are known. For (i), $\theta_{ij} = 71.57^\circ$. Note that, the individual dipoles do not make a uniform angle with respect to each other and thus $\theta_{ij}$ is not a uniquely defined angle due to relaxation in the optimized structure. This is true for all the real molecular architectures in calix[n]arenes. However, $\theta_{ij}$ does provide a very simple ''rule of thumb'' parameter for defining the cone angle and the dipole interaction for such otherwise complicated geometries.

For a more conclusive comparison of the evolution of the 1st hyperpolarizability with respect to the interdipolar angle, the magnitude of $\beta$ is studied with the increase in the interdipolar angle, $\theta_{ij}$. This is done by removing the

–$CH_2$–$CH_2$–$CH_2$– connectors between the chromophores and then flattening the calix[3]arene as was done for the parallel $(HF)_3$ case. The profile shows that $\beta_{calix[3]arenes}$ has a monotonic decay with the increase in the interdipolar angle and decays to zero at $\theta = 120$. It is very interesting to note that similar features are observed also for our $(HF)_3$ model.

For high NLO responses, the inter-molecular conformation of the dipoles should be parallel or almost parallel. To trace real molecular systems where such an orientation is possible, a search was carried out using the keyword 'calix[3]arene' in the Cambridge Structural Database[82] (CSD version, 5.25, November 2003 release). Structures of low quality ($R >$ 10%), disordered or in which the position of H atoms have not been determined, were excluded. A total of 4 structures were reprieved. Of these, two of the structures, CSD code: DIPWEE[83] and QETWAN[84] maintain a parallel-like orientation of the monomer chromophores, however for two entirely different reasons. DIPWEE has a large cavity size that incorporates a fullerene which prevents crossover to the frustrated dipolar form. However, due to the large cavity, it gives rise to a large cone-angle conformation. From the analysis based on the $(HF)_3$ geometry, it is clear that, systems with large cone angles are not suitable for efficient NLO applications.

QETWAN, on the other hand, is the simplest and yet extremely interesting. The structure has been shown in Fig. 14(iii). It has all the three individual chromophores in the same parallel orientation. The fourth chromophore is functionalized at the *meta*- positions such that it acts as a stitch for the rest of the three and forces a parallel orientation for the dipoles. The compound is found to possess highest magnitude of the 1st hyperpolarizability among all the calix[3]arene systems discussed ($\beta$ = 32076.64 au).

### 3.5 Odd–even oscillations in NLO of alkyl bridged dipolar chromophores

From the above discussion on the NLO properties of aggregates of chromophores connected through alkyl bridges, it is clear that the exciton theory is applicable to a reasonable extent for such cases. These alkyl bridges, in fact, act as harmless stitches, but since they are flexible, lead to many different orientations in the dipoles. The NLO responses of these orientations would be expected to be different. For a clear understanding of the stability of such specific orientations, the NLO properties of a few dipolar chromophores are calculated. These chromophores are separated by an alkyl bridge. The number of alkyl groups is varied to obtain a quantitative estimation of the orientation of the dipoles together with its effect on NLO properties of the system. Since dipole orientations would be strongly dependent on the conformations of the intervening methylene groups, the overall dipole moment is expected to show odd–even oscillations with the number of methylene groups.[85] Such odd–even oscillations are well-known in the literature for many physical properties like the melting points of organic solids[86] and the orientation of alkanethiols in self-assembled monolayers (SAMs).[87] Also, there have been recent experimental reports of odd–even oscillations in NLO properties of organic molecules similar to those discussed here[88] and even in different molecular systems.[89]

The oscillations in the physical properties such as melting point are generally understood on the basis of packing efficiencies in the van der Waals solids. The alkanes with odd-numbers of carbon atoms are packed less orderly than their even counterparts. However, oscillations in the electrical properties like hyperpolarizabilities are difficult to understand as they are very sensitive to both the nature of ground state and excited states. To understand the relationship between SHG coefficients and the geometrical orientations of the intervening methylene groups, we consider a set of molecular systems as shown in Fig. 15(A). All the geometries have been optimized using the AM1 parameterized Hamiltonian available in the Gaussian 03 set of codes. Some of the compounds (with smaller alkyl units) have already been synthesized in good yields and are well characterized, although, single crystalline forms are not available. The geometries obtained by the AM1 calculations have been compared with those obtained using the DFT based methods at the B3LYP/6-31G+(d,p) level for the smaller sized chromophore with $n = 2$. It is found that the geometries obtained by both the methods have similar bond lengths and bond angles. To further verify that the geometries do correspond to the global minima, the geometry for the experimentally synthesized molecule: 4,4′-diamino-2,2′-dinitrodiphenylmethane[90] is also optimized. For this molecule as well, the geometry and the interdipolar angle is similar to that considered in the present study.

R–$CH_2$–$CH_2$–R, R = Ph–N=N–Ph–$NO_2$, is the simplest symmetric case which can be considered to understand the conformational orientations, as shown in Fig. 15(B). Rotation along the central C–C bond produces different conformations. For a torsional angle, $\phi = 0$, the situation corresponds to an eclipsed geometry while for $\phi = 180$, the conformation is staggered. In Fig. 16, the potential energy profile for the system with an increase in torsional angle is plotted. The most stable point in the potential energy surface (PES) corresponds to $\phi = 180$ (staggered orientation in the dipoles) while the most unstable case is for $\phi = 0$ (the eclipsed form). Also, there exists a local minima between $\phi = 60$ and 80 and a local maxima at

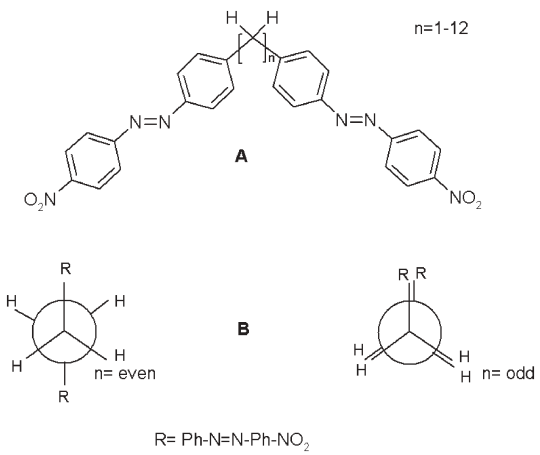


**Fig. 15** (A) Molecular structure of the system considered. (B) Orientation of the dipoles for odd and even chains.

 

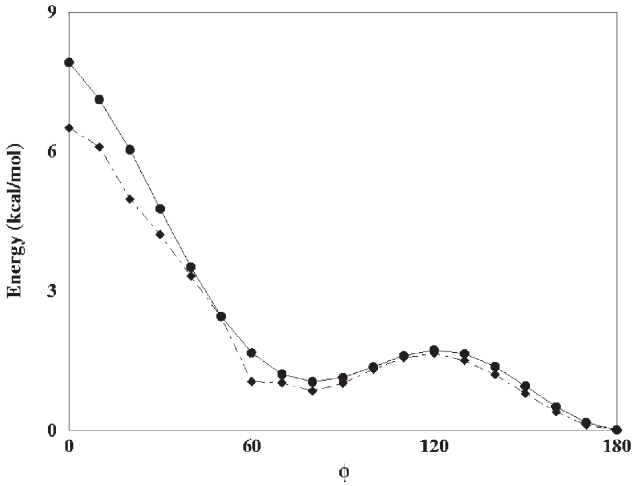


**Fig. 16** Potential energy (in kcal $mol^{-1}$) as a function of twist along the central C–C single bond: for $n = 2$, solid line (circles) and $n = 12$, dashed line (diamond).

$\phi = 120$. This is similar to the *gauche butane* interaction well-known in the literature.[91,92] This arises due to the stronger non-bonding interaction between R and H at an angle of $\phi = 120$, compared to the weak R,R interaction in the gauche form at $\phi \approx 60$.

For $n = 2$, the energy difference between the staggered and eclipsed form is 8 kcal $mol^{-1}$ while that between the staggered and the gauche form is 1.04 kcal $mol^{-1}$. For comparison, the differences are 4.4–6.1 kcal $mol^{-1}$ and 0.9 kcal $mol^{-1}$ respectively for butane. For a longer chain however, since there are more numbers of $CH_2$ groups, the degrees of freedom are much larger, allowing it to be in a state of random relaxed geometry without much constraints. In the same figure (Fig. 16), the PES for the longest chain considered in the work: $n = 12$ is also plotted. Note that, for such a large methylene bridge, there is no well-defined torsional angle parameter. However, for the sake of comparison, the central C–C bond, C(6)–C(7) is twisted. It has a lower energy difference between the staggered and eclipsed form (6.5 kcal $mol^{-1}$) and between the staggered and gauche form (0.84 kcal $mol^{-1}$), as expected.

For both $n = 2$ and $n = 12$, the energy difference between the eclipsed and the staggered forms are more than the thermal energy at room temperature (0.6 kcal $mol^{-1}$). The staggered form is the lowest energy orientation for all the systems in the $n$ = even cases. However, since the gauche conformation lies at a local minima, for longer chains, this conformational form becomes thermally accessible. A gauche form is interesting because it induces helicity in a linear chain. Such helical chains being chiral also exhibit good NLO responses for the even chains.[93–95]

The odd-chains however, show remarkable contrast. For the odd-chains, the favorable arrangement corresponds to an eclipsed orientation for the dipoles. This is explicitly shown in Fig. 15(B). One can understand this phenomenon from the simple fact that all the alkyl units being in an $sp^3$ environment introduce staggered geometry for all central units but eclipsed orientation between the extreme ends where the dipoles are located. So, the odd-chains will have a staggered orientation for the dipoles. For the even chains, however, there is no such frustration in the dipole orientations and all the units including the end dipoles remain staggered. Such a remarkable variation between the eclipsed and staggered conformation can be achieved by only changing the number of spacers between the dipoles.

The even chains have very little dipole moment ($\approx$3 D) while the odd ones have much higher dipole moment ($\approx$45 D). The dipole moment for the single molecule, Ph–N=N–Ph–$NO_2$ is calculated as, $\mu_G \approx 39.20$ D. For a perfect parallel arrangement in the dipoles, the classical non-interacting picture predicts the total dipole moment as $2\times$ single chromophore value for parallel arrangement and 0 for a perfect anti-parallel arrangement. While, for the even spacers the dipole moments are nearer to zero, the odd-spacers show much smaller value from the classical result of twice the single chromophore value. Such a trend can be easily understood: for the even chains, the dipoles are staggered and almost perfectly anti-parallel, however, for the odd chains, even though the orientations are eclipsed, the dipoles are not exactly parallel because of the $sp^3$ hybridization along the alkyl principle axis. It is straightforward to calculate the angle ($\phi$) in which the dipoles are out of phase, using the classical dipole addition formula: $\mu_{eff}^2 = \mu_1^2 + \mu_2^2 + 2\mu_1\mu_2\cos\phi$. $\phi$ is calculated as 110° for the odd chains. Note that, although a classical dipole expression is used to find the phase angle, it comes out as a good assumption as the saturated $CH_2$ groups have very little electronic coupling with the $\pi$-electrons in either ends of the bridge. For example, the actual angle for the optimized molecule with $n = 3$ is 112°. The alkyl units basically act as a stitch between the two dipoles.

With the increase in the number of alkyl units, the distance between the dipoles increases. But, the distance between the even dipoles is more than their odd counterparts as the even ones have a centrosymmetric arrangement which increases their interchromophore distances. Thus, the end-to-end distance between the dipoles also exhibit an odd–even effect (Fig. 17 (a)). For each even distance, $\beta$ is smaller and for each odd distance, $\beta$ is larger. Fig. 17 (b) shows the variation in the 1st hyperpolarizability, $\beta$, with respect to the number of $CH_2$ units. Very similar to that for the ground state dipole moment, $\beta$ also shows a very prominent odd-even oscillation. For odd chain, $\beta \approx 700$ while the even chain have $\beta \approx 80$ (in units of $10^{-30}$ esu). The calculations are based on a CI basis with its dimension varying till a proper convergence is reached.[85]

Within the framework of the two-state model, the SHG coefficient is directly proportional to the oscillator strength and the dipole moment difference and is inversely proportional to the optical gap. Thus, any phenomenon that decreases the gap or increases the dipole moment difference between the ground and the excited state or increases the oscillator strength will enhance $\beta$. The calculations show that both the optical gap ($\delta E$) as well as oscillator strengths almost remain the same for the even and odd chromophores. Thus, the only factor that governs such an odd–even oscillation is the $\Delta\mu$. Fig. 17(c) shows the variation of $\Delta\mu$ with increase in the spacer length. One can clearly see the odd–even variation in $\Delta\mu$ similar to that observed for $\beta$. This is to say that the excited state

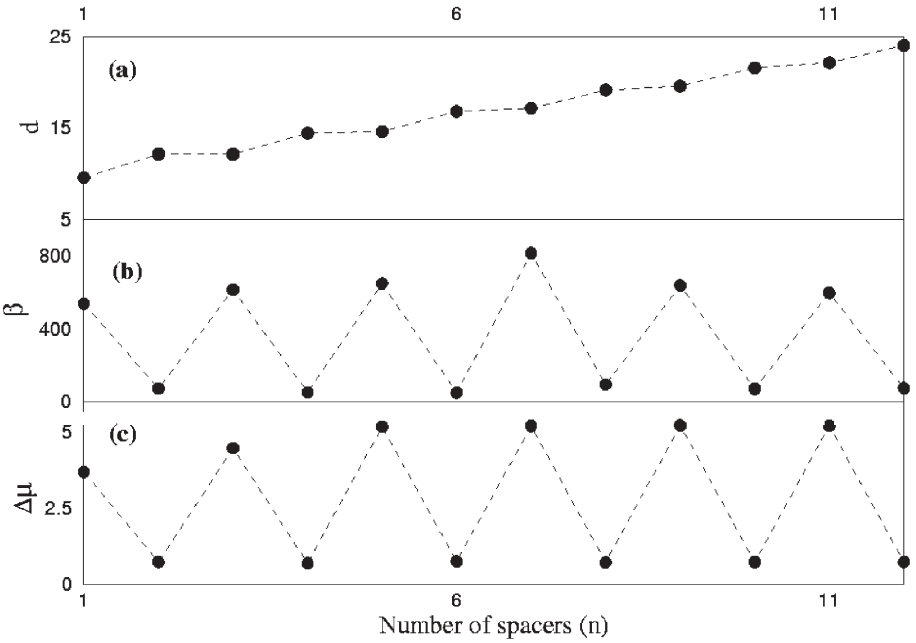


**Fig. 17** (a) Variation of interchromophore distance, $d$ (in Å), (b) 1st hyperpolarizability $\beta$ (in units of $10^{-30}$ esu), (c) difference between the ground state and the excited state dipole moment, $\Delta\mu$ (in Debye) with the increase in the spacers length, $n$.

polarization has a strong dependence on the interchromophoric arrangement.

From the present work it is clear that this phenomenon of odd–even fluctuation in NLO properties is different from the variation of the physical properties like melting point in organic solids that have their origin in the van der Waal's interactions among the solids where crystal packing is the most important parameter. The energy analysis for the potential energy of twisting along the single bond shows that although the staggered form is the most stable geometry for the even chains, however, a thermally allowed local minima exists between $\phi = 60$ and $\phi = 80$, corresponding to the gauche form that will lead to a helical chain. For example, we find that for every 100 molecules in the staggered form, there are 18 molecules in the gauche form (Boltzmann distribution) and even for the $n = 2$ case, the Boltzmann weighted average 1st hyperpolarizability, $\beta$ has a magnitude of $160.8 \times 10^{-30}$ esu. In the solid state due to environment effects, the possibility of existence of such a helical form (local minima) exists. As a result, for the even chains although a global minima form ensures $\beta$ to be very small, supramolecular effects as in thin-films will introduce appreciable $\beta$.

This phenomenon is essentially a consequence of the interactions in a single alkyl chain. In crystals or thin films, intermolecular interactions will be important and packing efficiency will ultimately decide the final geometries. But, the fact that a simple theory based on intramolecular interactions can capture this effect indicates that at least, for these molecules, intermolecular interactions are not very strong.

## 4 Summary and future prospects

There have been major advances in the construction, design and performance of NLO materials in the last couple of years. New theoretical formalisms have been developed for capturing essentials of novel π-conjugated organic systems which have helped in understanding the geometric and electronic features leading to highly effective NLO applications. A major stress for theoretical research is directed towards an atomistic understanding of the intermolecular forces in molecular aggregates and the collective behavior of the molecules under various packing densities and with different external fields.

Through proper fine-tuning of the intermolecular interactions, it has been possible to design materials wherein non-centrosymmetricity can be preserved. For example, selection of chromophores with moderate H-bonding interactions and moderate dipolar strengths would arrange the molecules in an head-to-tail arrangement. However, very strong H-bonding interactions would lead to the formation of cyclic clusters with high intermolecular D–H…A connectivity with eventual centrosymmetricity. Similarly, selection of very strong dipolar chromophores may make the aggregate ineffective through anti-parallel π-stacking interactions. In fact, the pro-typical NLO active urea crystal is suitable because both dipolar interactions as well as the H-bonding forces are moderate. In this context, one future direction will be to modify the interactions in derivatives of urea to further enhance the desired and effective intermolecular interactions. For the cases of dipolar molecules connected by flexible alkane bridges, careful synthesis of molecules with odd numbers of alkane spacers within the chromophores will lead to large NLO responses compared to the cases with even numbers of spacers. In confined dipolar environments like calix[n]arenes, one can stabilize the highly polarizable *all-up* conformers through fused bridging of the chromophores that prevent relaxation of the aggregates into centrosymmetric forms. Another possibility to enhance the NLO properties in calix[n]arenes will be to trap specific cations and anions within the cavities that lead to

 

enhanced charge transfer interactions between the π-electrons of the calix[n]arenes and the guest ions. This specific 'host–guest' chemistry may lead to novel NLO activities.

Additionally, apart from selection of dipolar molecules, a major goal will be to utilize octupolar molecules and arrange then in a way to achieve the maximum possible acentricity. H-bonds being strongly directional, have the potential to arrange such molecules in one-dimensional networks.

A major bottleneck for the industrial applications of the π-conjugated organic materials is their low-thermal stability as compared to the inorganic compounds. The last few years have witnessed active research in the synthesis of hybrid organic–inorganic materials, particularly through the solvothermal route.[96] These inorganic coordination polymers have extended structures which are connected through aromatic templates. The stability of these materials are as large as conventional inorganic materials, while their polarizations are much larger due to the delocalized π-electrons in the organic moieties. Many of these materials crystallize in acentric point-group and have NLO activities that are orders of magnitude larger than urea. In a similar context, crystals of organometallic compounds also exhibit large NLO activities.[97]

In this review, based on computational studies on finite-sized aggregates of experimentally realizable systems, we have comprehensively demonstrated the importance of cooperative interactions in controlling the 1st hyperpolarizabilities in multimolecular aggregates. We have emphasised the role of weak supramolecular forces in defining the SHG responses in molecular assemblies. The approach taken here is based on direct quantum chemical calculations of selected molecules and aggregates, variations of geometry to identify specific intermolecular interactions, and to analyse them based on molecular excitons. We believe that our review will serve as a guide for the design of materials exhibiting large 1st hyperpolarizabilities wherein the molecules are oriented in their most favourable arrangements.

## Acknowledgements

We thank Professors S. Ramasesha, T. P. Radhakrishnan, P. K. Das, P. Ray, Anna Painelli and B. Champagne for lively discussions on the fascinating area of supramolecular aspects of SHG. SKP thanks CSIR and DST, of the Government of India, for the research grants. AD thanks CSIR-India for the Senior research fellowship.

## References

1 (*a*) P. N. Prasad and D. J. Williams, *Introduction to Nonlinear Optical Effects in Molecules and Polymers*, Wiley, New York, 1991; (*b*) S. P. Karna and A. T. Yeates, *Nonlinear Optical Materials*, ACS Symposium Series, Washington DC, 1996.
2 *Optical Nonlinearities in Chemistry*, ed. D. M. Burland, *Chem. Rev.*, 1994, **94**, p. 1.
3 T. J. Marks and M. A. Ratner, *Angew. Chem., Int. Ed. Engl.*, 1995, **34**, 155.
4 (*a*) A. J. Heeger, S. Kivelson, J. R. Schrieffer and W.-P. Su, *Rev. Mod. Phys.*, 1988, **60**, 781; (*b*) M. Wohlgenannt, K. Tandon, S. Mazumdar, S. Ramasesha and Z. V. Vardeny, *Nature*, 2001, **409**, 494; R. S. Kohlman, A. Zibold, D. B. Tanner, G. G. Ihas, T. Ishiguro, Y. G. Min, A. G. MacDiarmid and A. J. Epstein, *Phys. Rev. Lett.*, 1997, **78**, 3915; (*c*) E. Hennebicq, G. Pourtois, G. D. Scholes, L. M. Herz, D. M. Russell, C. Silva, S. Setayesh, A. C. Grimsdale, K. Mllen, J.-L. Brdas and D. Beljonne, *J. Am. Chem. Soc.*, 2005, **127**, 4744; (*d*) K. S. Narayan and N. Kumar, *Appl. Phys. Lett.*, 2001, **79**, 1891.
5 K. V. Katti, K. Raghuraman, N. Pillarsetty, S. R. Karra, R. J. Gulotty, M. A. Chartier and C. A. Langhoff, *Chem. Mater.*, 2002, **14**, 2436.
6 J. D. Augspurger and C. E. Dykstra, *Int. J. Quantum Chem.*, 1992, **43**, 135.
7 L. Jensen, P.-O. Astrand, A. Osted, J. Kongsted and K. V. Mikkelsen, *J. Chem. Phys.*, 2002, **116**, 4001.
8 H. E. Katz, L. Wilson William and G. Scheller, *J. Am. Chem. Soc.*, 1994, **116**, 6636.
9 H. E. Katz, G. Scheller, T. M. Putvinski, M. L. Schilling, W. L. Wilson and C. E. D. Chidsey, *Science*, 1991, **254**, 1485.
10 (*a*) *Nonlinear optical properties of organic molecules and crystals*, ed. D. S. Chemla and J. Zyss, Academic Press., 1987; (*b*) J. Zyss, *J. Chem. Phys.*, 1993, **98**, 6583; (*c*) C. Fave, M. Hissler, K. Senechal, I. Ledoux, J. Zyss and R. Reau, *Chem. Commun.*, 2002, **16**, 1674.
11 (*a*) S. Philip Anthony, K. Basavaiah and T. P. Radhakrishnan, *Cryst. Growth Des.*, 2005, **5**, 1831; (*b*) K. Srinivas, S. Sitha, V. J. Rao, K. Bhanuprakash, K. Ravi Kumar, S. Philip Anthony and T. P. Radhakrishnan, *J. Mater. Chem.*, 2005, **15**, 965; (*c*) J. M. Cole, R. C. B. Copley, G. J. McIntyre, J. A. K. Howard, M. Szablewski and G. H. Cross, *Phys. Rev. B: Condens. Matter*, 2002, **65**, 125107.
12 (*a*) S. Debrus, M. K. Marchewka, J. Baran, M. Drozd, R. Czopnik, A. Pietraszko and H. Ratajczak, *J. Solid State Chem.*, 2005, **178**, 2880; (*b*) H. Ratajczak, J. Baran, A. J. Barnes, J. Barycki, S. Debrus, Z. Latajka, M. May and A. Pietraszko, *J. Mol. Struct.*, 2001, **596**, 17; (*c*) V. M. Chapela, M. J. Percino, A. Jimnez, R. Ortega-Martnez, C. A. Escalante and C. Rodrguez de Barbarn, *J. Mol. Struct.*, 2003, **648**, 115; (*d*) T. Pal, T. Kar, G. Bocelli and L. Rigi, *Cryst. Growth Des.*, 2003, **3**, 13; (*e*) M. K. Marchewka, S. Debrus and H. Ratajczak, *Cryst. Growth Des.*, 2003, **3**, 587.
13 (*a*) S. Di. Bella, M. A. Ratner and T. J. Marks, *J. Am. Chem. Soc.*, 1992, **114**, 5842; (*b*) S. Keinan, M. A. Ratner and T. J. Marks, *Chem. Mater.*, 2004, **16**, 1848.
14 V. Moliner, P. Escribano and E. Peris, *New J. Chem.*, 1998, 387.
15 K. Wu, J. G. Snijders and C. Lin, *J. Phys. Chem. B*, 2002, **106**, 8954.
16 J. A. R. P. Sarma, J. L. Rao and K. Bhanuprakash, *Chem. Mater.*, 1995, **7**, 1843.
17 (*a*) M. Guillaume, E. Botek, B. Champagne, F. Castet and L. Ducasse, *Int. J. Quantum Chem.*, 2002, **90**, 1378; (*b*) F. Castet and B. Champagne, *J. Phys. Chem. A*, 2001, **105**, 1366.
18 B. Champagne and D. M. Bishop, *Adv. Chem. Phys.*, 2003, **126**, 41.
19 L. Jensen, P.-O. Astrand, A. Osted, J. Kongsted and K. V. Mikkelsen, *J. Chem. Phys.*, 2002, **116**, 4001.
20 (*a*) J. D. Augspurger and C. E. Dykstra, *Int. J. Quantum Chem.*, 1992, **43**, 135; (*b*) G. Maraoulis, *J. Chem. Phys.*, 2000, **113**, 1813.
21 S. K. Pati, S. Ramashesha, Z. Shuai and J. L. Bredas, *Phys. Rev. B: Condens. Matter*, 1999, **59**, 14827.
22 R. Custelcean, M. G. Gorbunova and P. V. Bonnesen, *Chem.–Eur. J*, 2005, **11**, 1459.
23 C.-R. Lee, T.-H. Tang, L. Chen and Y. Wang, *Chem.–Eur. J*, 2003, **9**, 3112.
24 N. Harada, Y. Takuma and H. Uda, *J. Am. Chem. Soc.*, 1978, **100**, 4029.
25 *Circular Dichroic Spectroscopy: Exciton Coupling in Organic Stereochemistry*, ed. K. Nakanishi, University Science Books, Mill Valley, CA, 1983.
26 G. D. Scholes, K. P. Ghiggino, A. M. Oliver and M. N. Paddon-Row, *J. Am. Chem. Soc.*, 1993, **115**, 4345.
27 (*a*) J. McCullough, *Chem. Rev.*, 1987, **87**, 811; (*b*) M. Kasha, *Rev. Mod. Phys.*, 1959, **31**, 162.
28 A. S. Davydov, *Theory of Molecular Excitons*, McGraw-Hill, New York, 1962.
29 H. Suzuki, *Electronic Absorption Spectra: Geometry of Organic Molecules*, Academic Press, New York, 1967.
30 (*a*) A. J. Stone, *The Theory of Intermolecular Forces*, Clarendon Press, Oxford, 2002; (*b*) D. A. McQuarrie and J. D. Simon, *Physical Chemistry*, University Science Books, Sausalito, CA, 1999.

31 (*a*) F. Terenziani and A. Painelli, *J. Lumin.*, 2005, **112**, 474; (*b*) A. Painelli and F. Terenziani, *J. Lumin.*, 2003, **139**, 779.
32 (*a*) F. Terenziani and A. Painelli, *Phys. Rev. B: Condens. Matter*, 2003, **68**, 1654051; (*b*) A. Painelli and F. Terenziani, *J. Am. Chem. Soc.*, 2003, **125**, 5624.
33 (*a*) A. Painelli, F. Terenziani, L. Angiolini, T. Benelli and L. Giorgini, *Chem.–Eur. J*, 2005, **11**, 6053; (*b*) F. Terenziani, O. Mongin, C. Katan, B. K. G. Bhatthula and M. B-Desce, *Chem.–Eur. J*, 2006, **12**, 3089; (*c*) F. Terenziani, M. Morone, S. Gmouh and M. B-Desce, *ChemPhysChem*, 2006, **7**, 537.
34 A. R. Leach, *Molecular Modelling: Principles and Applications*, Pearson Education Ltd, Essex, UK, 1996.
35 A. K. Rappe and C. J. R. Casewit, *Molecular Mechanics across Chemistry*, University Science Books, Sausalito, CA, 1997.
36 F. Jensen, *Introduction to Computational Chemistry*, Wiley, Chichester, 1999.
37 (*a*) T. Steiner, *Angew. Chem., Int. Ed.*, 2002, **41**, 48; (*b*) G. R. Desiraju and T. Steiner. *The weak hydrogen bond in structural chemistry and biology*, Oxford University Press, Oxford, UK, 1999.
38 S. Scheiner, *Hydrogen Bonding: A theoretical perspective*, Oxford University Press, 1997.
39 (*a*) W. Kohn, Y. Meir and D. E. Makarov, *Phys. Rev. Lett.*, 1998, **80**, 4153; (*b*) J. M. Perez-Jorda and A. D. Becke, *Chem. Phys. Lett.*, 1995, **233**, 134.
40 Y. Andersson, D. C. Langreth and B. I. Lundqvist, *Phys. Rev. Lett.*, 1996, **76**, 102.
41 S. Tsuzuki, K. Honda, T. Uchimura and M. Mikami, *J. Chem. Phys.*, 2004, **120**, 647.
42 S. Grimme, *J. Comput. Chem.*, 2004, **25**, 1463.
43 Q. Wu and W. Yang, *J. Chem. Phys.*, 2002, **116**, 515.
44 M. Elstner, P. Hobza, T. Frauenheim, S. Suhai and E. Kaxiras, *J. Chem. Phys.*, 2001, **114**, 5149.
45 E. Brouyère, A. Persoons and J. L. Brédas, *J. Phys. Chem. A*, 1997, **101**, 4142.
46 P. C. Ray and J. Leszczynski, *Chem. Phys. Lett.*, 2006, **419**, 578.
47 W.-D. Cheng, D.-S. Wu, H. Zhang, X.-D. Li, D.-G. Chen, Y.-Z. Lang, Y.-C. Zhang and Y.-J. Gong, *J. Phys. Chem. B*, 2004, **108**, 12658.
48 (*a*) S. F. Boys and F. Bernardi, *Mol. Phys.*, 1970, **19**, 553; (*b*) D. W. Scwenke and D. G. Truhler, *J. Chem. Phys.*, 1985, **82**, 2418.
49 M. J. Frisch, G. W. Trucks, H. B. Schlegel, G. E. Scuseria, M. A. Robb, J. R. Cheeseman, V. G. Zakrzewski, J. A. Montgomery, Jr., R. E. Stratmann, J. C. Burant, S. Dapprich, J. M. Millam, A. D. Daniels, K. N. Kudin, M. C. Strain, O. Farkas, J. Tomasi, V. Barone, M. Cossi, R. Cammi, B. Mennucci, C. Pomelli, C. Adamo, S. Clifford, J. Ochterski, G. A. Petersson, P. Y. Ayala, Q. Cui, K. Morokuma, P. Salvador, J. J. Dannenberg, D. K. Malick, A. D. Rabuck, K. Raghavachari, J. B. Foresman, J. Cioslowski, J. V. Ortiz, A. G. Baboul, B. B. Stefanov, G. Liu, A. Liashenko, P. Piskorz, I. Komaromi, R. Gomperts, R. L. Martin, D. J. Fox, T. Keith, M. A. Al-Laham, C. Y. Peng, A. Nanayakkara, M. Challacombe, P. M. W. Gill, B. G. Johnson, W. Chen, M. W. Wong, J. L. Andres, C. Gonzalez, M. Head-Gordon, E. S. Replogle and J. A. Pople, *GAUSSIAN 98 (Revision A.10)*, Gaussian, Inc., Pittsburgh, PA, 2001.
50 (*a*) J. Ridley and M. C. Zerner, *Theor. Chim. Acta*, 1973, **32**, 111; (*b*) A. D. Bacon and M. C. Zerner, *Theor. Chim. Acta*, 1979, **53**, 21.
51 R. J. Buenker and S. D. Peyerimhoff, *Theor. Chim. Acta*, 1974, **35**, 33.
52 Z. Shuai, D. Beljonne and J. L. Bredas, *J. Chem. Phys.*, 1992, **97**, 1132.
53 D. Beljonne, Z. Shuai, J. Cornil, D. dos Santos and J. L. Bredas, *J. Chem. Phys.*, 1999, **111**, 2829.
54 (*a*) S. Ramasesha and Z. G. Soos, *Chem. Phys. Lett.*, 1988, **153**, 171; (*b*) Z. G. Soos and S. Ramasesha, *J. Chem. Phys.*, 1989, **90**, 1067.
55 (*a*) S. Ramasesha, Z. Shuai and J. L. Bredas, *Chem. Phys. Lett.*, 1995, **245**, 224; (*b*) I. D. L. Albert and S. Ramasesha, *J. Phys. Chem.*, 1990, **94**, 6540; (*c*) S. Ramasesha and I. D. L. Albert, *Phys. Rev. B: Condens. Matter*, 1990, **42**, 8587.
56 S. K. Pati, T. J. Marks and M. A. Ratner, *J. Am. Chem. Soc.*, 2001, **123**, 7287.
57 H. A. Kurtz, J. J. P. Stewart and K. M. Dieter, *J. Comput. Chem.*, 1990, **11**, 82.
58 K. B. Sophy and S. Pal, *J. Chem. Phys.*, 2003, **118**, 10861.
59 L. D. Freo, F. Terenziani and A. Painelli, *J. Chem. Phys.*, 2002, **116**, 755.
60 A. Datta and S. Pal, *THEOCHEM*, 2005, **715**, 59.
61 (*a*) J. Mack, Y. Asano, N. Kobayashi and M. J. Stillman, *J. Am. Chem. Soc.*, 2005, **127**, 17697; (*b*) J.-S. K. Yu, W.-C. Chen and C.-H. J. Yu, *Phys. Chem. A.*, 2003, **107**, 4268.
62 (*a*) J. L. Oudar and D. S. Chemla, *J. Chem. Phys.*, 1977, **66**, 2664; (*b*) J. L. Oudar, *J. Chem. Phys.*, 1977, **67**, 446.
63 A. Datta and S. K. Pati, *J. Chem. Phys.*, 2003, **118**, 8420.
64 F. Spano, J. Kuklinski and S. Mukamel, *Phys. Rev. Lett.*, 1990, **65**, 211; V. Kamalov, I. A. Struganova and K. Yoshihara, *J. Chem. Phys.*, 1996, **100**, 8640.
65 S. Yitzchaik, G. Berkovic and V. Krongauz, *Adv. Mater.*, 1990, **2**, 33; S. Yitzchaik, S. Di Bella, P. M. Lundquist, G. K. Wong and T. J. Marks, *J. Am. Chem. Soc.*, 1997, **119**, 2995.
66 (*a*) J. Zyss, J. F. Nicould and M. J. Coquillay, *J. Chem. Phys.*, 1984, **81**, 4160; (*b*) B. R. Grubbs, S. R. Marder and J. W. Perry, *Chem. Mater.*, 1991, **3**, 3.
67 J. D. Bierlein, L. K. Cheng, Y. Wang and W. Tam, *Appl. Phys. Lett.*, 1990, **56**, 423.
68 (*a*) K. Morokuma, *Acc. Chem. Res.*, 1977, **10**, 294; (*b*) K. Morokuma and K. Kitaura, *Chemical Applications of Electrostatic Potentials*, ed. P. Politzer and D. G. Truhlar, Plenum Press, NY, 1981, pp. 215–242.
69 S. R. Marder, J. W. Perry and C. P. Yakymyshyn, *Chem. Mater.*, 1994, **6**, 1137.
70 A. Datta and S. K. Pati, *THEOCHEM*, 2005, **756**, 97.
71 R. Sudharsanam, S. Chandrasekaran and P. K. Das, *J. Mol. Struct.*, 2003, **645**, 51.
72 H. Jiang, A. K. Kakkar, A.-M. Lebuis, H. Zhou and G. K. Wong, *J. Mater. Chem.*, 1996, **6**, 1075.
73 A. Datta and S. K. Pati, *J. Phys. Chem. A*, 2004, **108**, 320.
74 (*a*) C. D. Gutsche, *Calixarenes Revisited*, Royal Society of Chemistry, Cambridge, UK, 1998; (*b*) A. Ikeda and S. Shinkai, *Chem. Rev.*, 1997, **97**, 1713.
75 (*a*) M. S. Wong, X. L. Zhang, D. Z. Chen and W. H. Cheung, *Chem. Commun.*, 2003, 138; (*b*) M. S. Wong, Z. H. Li and C. C. Kwok, *Tetrahedron Lett.*, 2000, **41**, 5719; (*c*) T. Gu, C. Bourgogne and J.-F. Nierengarten, *Tetrahedron Lett.*, 2001, **42**, 7249.
76 (*a*) E. Kelderman, L. Derhaeg, G. J. T. Heesink, W. Verboom, J. F. J. Engbersen, N. F. van Hulst, A. Persoons and D. N. Reinhoudt, *Angew. Chem., Int. Ed. Engl.*, 1992, **31**, 1075; (*b*) F. Vocanson, P. S. Ferrand, R. Lamartine, A. Fort, A. W. Coleman, P. Shahgaldian, J. Mugnier and A. Zerroukhi, *J. Mater. Chem.*, 2003, **13**, 1596; (*c*) T. Verbiest, S. Houbrechts, M. Kauranen, K. Clays and A. Persoons, *J. Mater. Chem.*, 1997, **7**, 2175.
77 (*a*) P. J. A. Kenis, O. F. J. Noordman, S. Houbrechts, G. J. van Hummel, S. Harkema, F. C. J. M. van Veggal, K. Clays, J. F. J. Engbersen, A. Persoons, N. F. van Hulst and D. N. Reinhoudt, *J. Am. Chem. Soc.*, 1998, **120**, 7875.
78 E. Brouyere and J. L. Bredas, *Synth. Met.*, 1995, **71**, 1699.
79 A. Datta and S. K. Pati, *Chem.–Eur. J*, 2006, **11**, 4961.
80 W. Chen, Z.-R. Li, D. Wu, Y. Li, C.-C. Sun, F. L. Gu and Y. Aoki, *J. Am. Chem. Soc.*, 2006, **128**, 1072.
81 P. D. J. Grootenhuis, P. A. Kollman, L. C. Groenen, D. N. Reinhoudt, G. J. van Hummel, F. Ugozzoli and G. D. Andreeti, *J. Am. Chem. Soc.*, 1990, **112**, 4165.
82 F. H. Allen, S. Bellard, M. D. Brice, B. A. Cartwright, A. Doubleday, H. Higgs, T. Hummelink, B. G. Hummelink-Peters, O. Kennard, W. D. S. Motherwell, J. Rodgers and D. G. Watson, *Acta. Crystallogr. Sect. B*, 1979, **35**, 2331.
83 K. Tsubaki, Y. Murata, K. Komatsu, T. Kinoshita and K. Fuji, *Heterocycles*, 1999, **51**, 2553.
84 T. Yamato, F. Zhang, H. Tsuzuki and Y. Miura, *Eur. J. Org. Chem.*, 2001, 1069.
85 A. Datta, S. K. Pati, D. Davis and K. Sreekumar, *J. Phys. Chem. A*, 2005, **109**, 4112.
86 Y. L. Slovokhotov, I. S. Neretin and J. A. K. Howard, *New J. Chem.*, 2004, **28**, 967.
87 (*a*) V. J. Angelico, S. A. Mitcell and V. H. Wysocki, *Anal. Chem.*, 2000, **72**, 2603; (*b*) D. M. Alloway, *J. Phys. Chem. B*, 2003, **107**, 11690.


 

88 S. K. Asha, K. Kavita, P. K. Das and S. Ramakrishnan, *Chem. Mater.*, 1999, **11**, 3352.
89 P. Gangopadhyay and T. P. Radhakrishnan, *Chem. Mater.*, 2000, **12**, 3362.
90 D. Bahulayan and K. J. Sreekumar, *J. Mater. Chem.*, 1999, **9**, 1425.
91 Jerry March. *Advanced Organic Chemistry: Reactions, Mechanisms and Structure*, John Wiley and Sons, 4th edn, 1992.
92 E. L. Eliel, *Stereochemistry of Carbon Compounds*, McGraw-Hill Inc, 1962.
93 P. Gangopadhyay and T. P. Radhakrishnan, *Angew. Chem., Int. Ed.*, 2001, **40**, 2451.
94 E. Botek, B. Champagne, M. Turki and J.-M. Andre, *J. Chem. Phys.*, 2004, **120**, 2042.
95 B. Philip and K. Sreekumar, *J. Poly. Sci. A, Poly. Chem.*, 2002, **40**, 2868.
96 (*a*) B. Lebeau, S. Brasselet, J. Zyss and C. Sanchez, *Chem. Mater.*, 1997, **9**, 1012; (*b*) L. Pan, X. Huang, J. Li, Y. Wu and N. Zheng, *Angew. Chem., Int. Ed.*, 2000, **39**, 527; (*c*) C. Serre and G. Frey, *J. Mater. Chem.*, 2002, **12**, 3053; (*d*) J.-min Shi, W. Xu, Q. yun Liu, F. Liu, Z. Huang, H. Lei, W.-t. Yu and Qi Fang, *Chem. Commun.*, 2002, 756; (*e*) E. Cariati, R. Ugo, F. Cariati, D. Roberto, N. Masciocchi, S. Galli and A. Sironi, *Adv. Mater.*, 2001, **13**, 1665.
97 (*a*) J. Qin, D. Liu, C. Dai, C. Chen, B. Wu, C. Yang and C. Zhan, *Coord. Chem. Rev.*, 1999, **188**, 23; (*b*) K. Snchal, L. Toupet, I. Ledoux, J. Zyss, H. L. Bozec and O. Maury, *Chem. Commun.*, 2004, 2180; (*c*) S. P. Anthony, P. Raghavaiah and T. P. Radhakrishnan, *Cryst. Growth Des.*, 2003, **3**, 631.